Published in American Journal of Science 302 : 517-547, 2002,
which should be used for any reference to this work

FLUID FLOW PATHWAYS ALONG THE GLARUS OVERTHRUST DERIVED FROM STABLE AND Sr-ISOTOPE PATTERNS

NICOLAS P. BADERTSCHER*, RAINER ABART**, MARTIN BURKHARD*,†,
and ANDREW McCAIG***

ABSTRACT. The Glarus thrust of the eastern Helvetic Alps has been proposed as a major pathway for metamorphic fluids expelled from the footwall during alpine deformation and prograde metamorphism. The stable isotope composition of calcite in a thin continuous calc-mylonite layer and gradients into the overlying Verrucano siltstones and underlying Flysch or carbonate are analyzed in detail. A regional scale map of the $\delta^{18}O$ composition of the calc-mylonite covering 25 kilometers east-west by 15 kilometers north-south is interpolated from 35 sampling sites with a total of over 700 samples. This map reveals a steep northward increase in $\delta^{18}O$ from 11 to 18 permil (SMOW), interpreted as an isotopic front within the southernmost 6 kilometers, and leveling out at about 20 permil farther north. Vertical profiles across the sharp thrust contact show significantly different isotopic fronts in the south, where the Verrucano Formation is thrust upon marine carbonates and in northern sites, where it rests on Tertiary Flysch.

Southern sites display steep continuous isotopic gradients over about 1 meter above the thrust, where both $\delta^{18}O$ and $\delta^{13}C$ decrease to background, Verrucano Formation values of 10 to 11 permil ($\delta^{18}O$ SMOW) and −6 permil ($\delta^{13}C$ PDB) respectively. Footwall carbonates are significantly depleted from their original value of about 26 permil within a zone of less than 10 meters below the thrust contact. The front geometry of $\delta^{13}C$ increasing from −2 to +2 permil downward within about 1 meter is much steeper than the one defined by $\delta^{18}O$.

Northern sites, in contrast, display distended isotopic alteration fronts upward into the Verrucano hangingwall, where higher than background values in $\delta^{18}O$ and $\delta^{13}C$ are found up to 15 meters and 6 meters above the thrust contact, respectively. No isotopic alterations could be detected within the footwall Flysch up to the thrust contact. The $^{87}Sr/^{86}Sr$ systematics has been observed on the centimeter to millimeter-scale in vertical profiles across the calc-mylonite in three southern sites. In each sample (slab), a topmost zone of slightly enriched, homogeneous $^{87}Sr/^{86}Sr$ values (0.709 to 0.712) is found within a zone of highly sheared and dynamically recrystallized yellow veins alternating with dark stylolite seams on the sub-millimeter scale. In two slabs, smooth vertical downward gradients to marine carbonate values (0.708) could be observed on the centimeter-scale.

Regional and local isotopic gradients are explained as exchange between the different rock reservoirs through the advection/diffusion/dispersion of fluids interacting in a regime of brittle/ductile deformation associated with >30 kilometers northward thrust translation. Different scenarios of fluid flow along and/or across the thrust plane are modeled using transport theory coupled with isotopic exchange reactions at an assumed temperature of 300°C.

Considerable amounts of externally derived ^{18}O-depleted, basement-derived fluids are required to explain the isotopic characteristics in the southern part of the thrust. A time integrated fluid flux (TIFF) of 4500 to 9100 m^3/m^2 is calculated for the channelized flow component along the thrust, far exceeding any cross-thrust component of downward fluid infiltration of 3.45 to 5.7 m^3/m^2. In northern sites, however, any potential thrust parallel fluid flow is obscured by a dominant component of upward, cross-thrust flow of fluids derived from compaction/dehydration of Flysch units in the immediate footwall. These calcite saturated fluids left their imprint in the hangingwall Verrucano Formation in the form of increasingly ^{13}C and ^{18}O depleted secondary calcite.

* Université de Neuchatel, Institut de Géologie, 11 Emile-Argand KP2, 2007 Neuchâtel, Switzerland
** Institut für Mineralogie und Petrologie, Universitaetsplatz 2, 8010 Graz, Austria
*** School of Earth Sciences, The University of Leeds, Leeds LS2 9JT, United Kingdom
† Corresponding author

INTRODUCTION

Faults and shear zones are believed to play a crucial role in the control of fluid flow in the upper and middle crust (Cox, 1987; Dipple and Ferry, 1992; Kerrich and others, 1984; McCaig, 1984). Thrust faults may channelize fluids (Fyfe and Kerrich, 1985; McCaig, 1989; Oliver, 1986; Yardley and Lloyd, 1995; Dipple and Ferry, 1992; Marquer and Burkhard, 1992) by enhancing permeability through the generation of micro-cracks during deformation at high fluid pressures (Cox and Etheridge, 1989; Etheridge and others, 1984; Etheridge, Wall, and Vernon, 1983; Knipe and McCaig, 1994; McCaig, Wickham, and Taylor, 1990; Oliver, 1996; Oliver, Valenta, and Wall, 1990). Fluid flow along thrusts has been the subject of many investigations in the last two decades and is well documented in many collision belts (Burkhard and Kerrich, 1988; Burkhard and others, 1992; Cathless, 1990; Crespo-Blanc and others, 1995; McCaig, Tritlla, and Banks, 2000; McCaig and others, 1995) as well as in accretionary prisms (Sample, 1996; Silver and others, 2000), where flow along faults best explains observed thermal and chemical anomalies.

High fluid pressure also plays an important role in the development of low angle thrust faults (Hubbert and Rubey, 1959) by lowering normal stress. Such a normal stress reduction has been proposed as a solution to the mechanical paradox of large overthrusts (Badertscher and Burkhard, 2001; Hsu, 1969; Price, 1988).

Isotopes in general, and stable isotopes of oxygen in particular, are a very powerful tool to study fluid-rock interaction, because oxygen is a major component of rocks and common geofluids. As a result, oxygen isotopes are sensitive tracers of interactions between fluids and rocks that are not in isotopic equilibrium with each other (Eppel and Abart, 1997; McCaig, 1997). Such a situation is likely to occur when isotopically distinct rock reservoirs are juxtaposed at a structural boundary. The situation of the Glarus thrust is ideal in this respect, as the three lithologies involved in the Glarus thrust system display very contrasting oxygen isotope compositions.

According to transport theory (Baumgartner and Rumble, 1988; Bickle and McKenzie, 1987), any original step-like isotope front in a rock system will be displaced by fluid transport as a sharp front in the direction of flow by a distance proportional to the total flux, if advection is the only effective process of flow. If the scale of diffusion and hydrodynamic dispersion is large compared to advection, initially sharp fronts may be dramatically broadened (Baker and Spiegelman, 1995; Bickle and McKenzie, 1987).

Distension of sharp fronts may also occur if the rate of fluid-rock reaction is slow compared to fluid infiltration velocities (Abart and Pozzorini, 2000; Abart and Sperb, 1997; Bowman, Willett, and Cook, 1994; Lassey and Blattner, 1988). Inversely, the shape of an observed isotope front constrains the direction of fluid flow, the time-integrated fluid fluxes, the mechanism of fluid transport and the original fluid compositions.

The Helvetic fold and thrust belt has been subject to several isotopic investigations of the fluid regimes during deformation (Burkhard and Kerrich, 1988; Crespo-Blanc and others, 1995; Kirschner, Masson, and Sharp, 1999; Marquer and Burkhard, 1992). All these studies found evidence for large-scale fluid flow along some thrust contacts. In a previous study of the Glarus overthrust, Burkhard and others (1992) discovered a conspicuous south-north increasing trend in the $\delta^{18}O$ composition of the calc-mylonite along the thrust fault (fig. 1). From cross-section balancing considerations it is clear that the Glarus thrust must extend backward to mid-crustal levels (Pfiffner, 1985). Burkhard and others (1992) and Bowman, Willett, and Cook (1994) interpreted this $\delta^{18}O$ trend as an isotope front due to the northward advection of ^{18}O depleted, externally derived fluids in a pre-existing carbonate along the thrust. Most

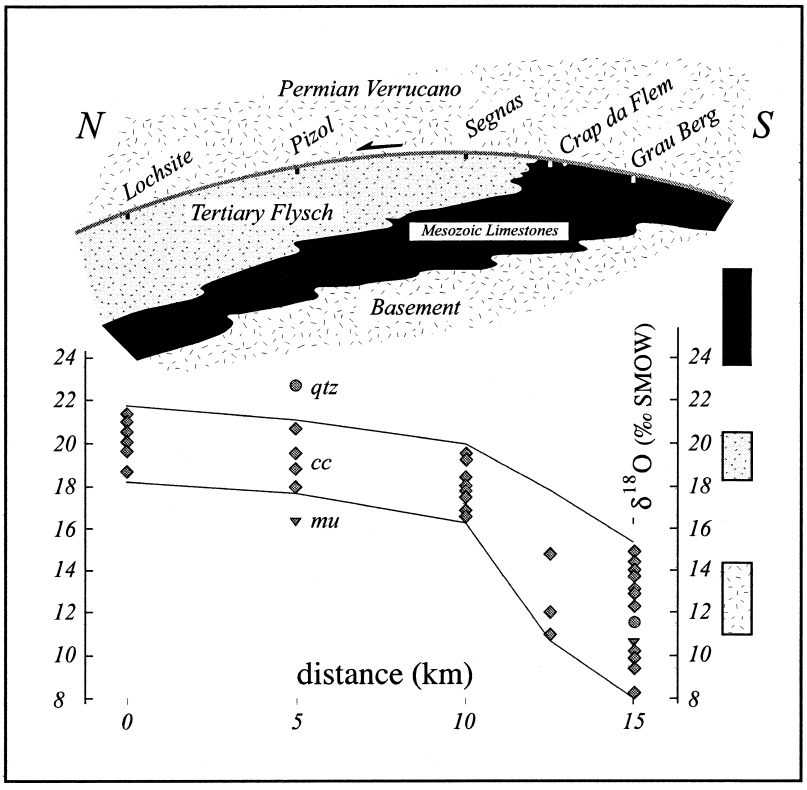

Fig. 1. Plot of calcite $\delta^{18}O$ values from the Lochsitenkalk mylonite on a schematic north-south cross section of the Glarus thrust. The range of whole rock isotopic composition for different potential fluid reservoirs is indicated to the right of the $\delta^{18}O$ scale using the corresponding shading (modified after Burkhard and Kerrich (1990)

likely these fluids were derived from devolatilization reactions in the basement farther south (Aar or Gotthard Massif, see fig.2). Bowman, Willett, and Cook (1994) applied transport theory to model the $\delta^{18}O$ data of the Glarus thrust. They treated the Glarus thrust as a 1-D system along which ^{18}O depleted fluids flowed northward, thereby displacing and broadening an initially sharp isotope front by advection and dispersion. The model of Bowman, Willett, and Cook (1994) suffers several weak points. First, they were obliged to use an unaltered initial $\delta^{18}O$ value of 20 permil for the pre-existing carbonate in order to obtain a reasonable fit with the data instead of the 25 to 26 permil value proposed by Burkhard and others (1992). Secondly, their model was built on a limited data set from the Lochsitenkalk mylonite only. Finally and most importantly at this time, no data about isotopic variations across the thrust were available.

The aim of this paper is to define the flow pattern associated with the Glarus thrust by considering isotopic variations along and across the Glarus overthrust through extended sampling. We start with the establishment of a detailed isotopic characterization of the calc-mylonite along the thrust on the km-scale. In addition, vertical profiles on the m-scale have been sampled in order to constrain the vertical flow components. $^{87}Sr/^{86}Sr$ data provide information about the influence of "basement" derived fluids. Together, these data define complex isotope fronts. Their shape and size is used to infer fluid flow parameters.

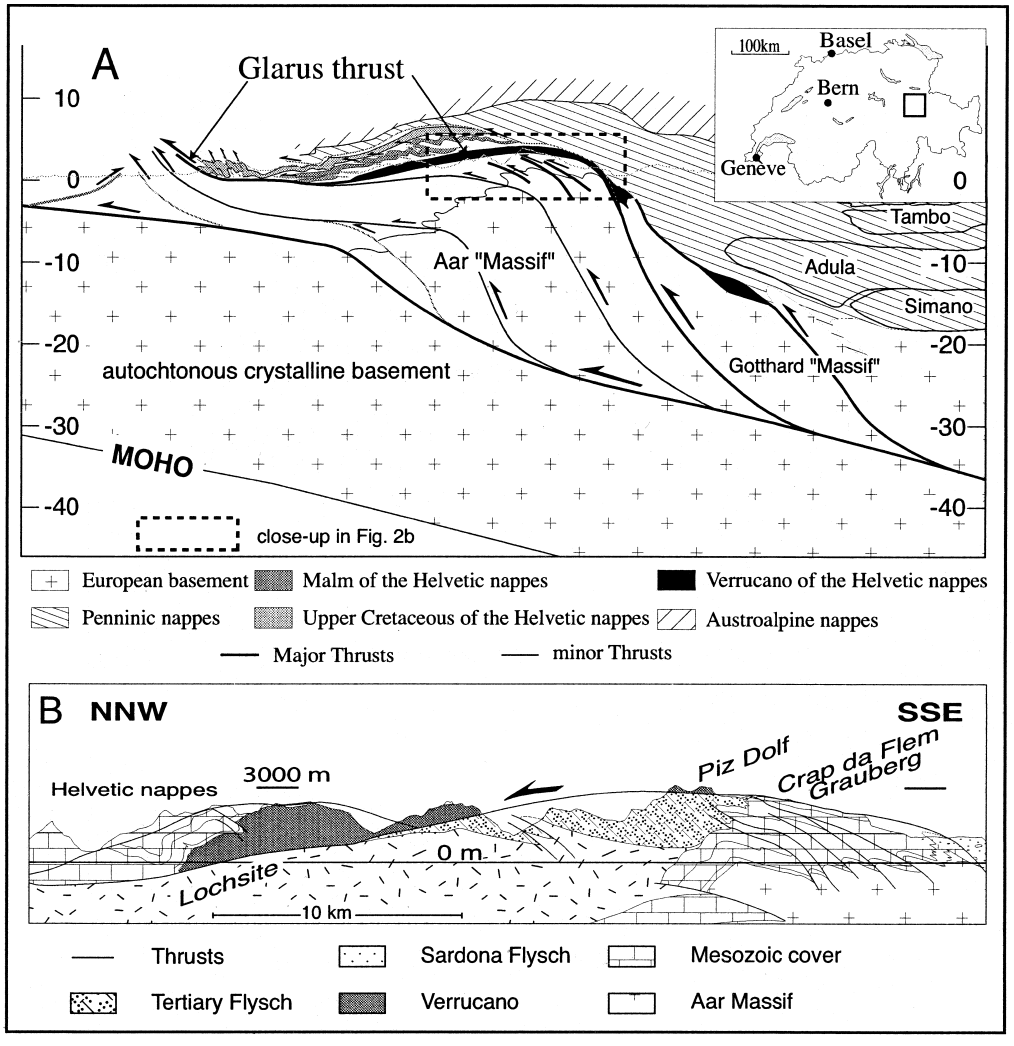

Fig. 2. (A) NNW-SSE crustal cross section through the eastern Alps of Switzerland (redrawn after cross section by Pfiffner (1993) and Schmid and others (1997). The accessible part of the Glarus overthrust is indicated within the box. (B) Cross section of the Glarus Alps in eastern Switzerland (according to Oberholzer, 1933). Some sampling sites are indicated.

GEOLOGICAL SETTING

In the Eastern Helvetic Alps of Switzerland (fig. 2), tectonic units are subdivided into a "Helvetic complex" above and an "Infrahelvetic complex" below the Glarus thrust (Pfiffner, 1981; Pfiffner, 1993). The Helvetic Glarus nappe comprises the Permian Verrucano Formation (VF), which consists of a clastic series of predominantly siltstones and shales with some conglomeratic units and rare volcanoclastic horizons overlain by a concordant Mesozoic series. The "Infrahelvetic" complex consists of a crystalline basement overlain by a parautochthonous sedimentary cover of Mesozoic carbonates and Tertiary Flysch with some allochthonous south Helvetic and Penninic (Sardona) Flysch (fig. 2B). The latter were emplaced upon the parautochthonous cover in early Oligocene times during the "Pizol phase" (Pfiffner, 1977). In a second,

main deformation stage (Calanda phase), the whole Infrahelvetic complex and Basement was intensely folded and imbricated. Final emplacement and thrusting of the Glarus nappe (Ruchi phase) post-dates these deformations (Pfiffner, 1977) in an out-of-sequence manner. Despite this out-of-sequence character, the Glarus overthust generally cuts up-section from south to north (fig. 2B). In the southernmost exposures, the Verrucano is thrust over parautochthonous Late Jurassic and Early Cretaceous limestones, whereas farther north it overlies a more than kilometer thick sequence of Flysch, consisting of marly shales, sandstones, and conglomerates (fig. 2B). An intermediate thin layer (<1 to 5 m thick) of intensively deformed calc-mylonite, the so-called Lochsitenkalk (LK), accommodated a large part of the 35 kilometers of thrust-translation towards the north (Schmid, 1975; Schmid, Boland, and Paterson, 1977).

Metamorphism ranges from anchizone in the north and in the footwall Flysch to lower greenschist facies in the south and in the hangingwall (Frey, 1988; Rahn and others, 1995) as determined from illite crystallinity, mineral parageneses, vitrinite reflectance, and fluid inclusions. The peak of this metamorphism post-dates the Calanda phase deformations (Groshong, Pfiffner, and Pringle, 1984) estimated at 30 to 25 Ma. The "anchizone-/epizone- boundary" is offset along the Glarus thrust by about 2 kilometers (Groshong, Pfiffner, and Pringle, 1984; Frey, 1988) as the result of post-peak-metamorphic thrusting between 25 and 20 Ma (Hunziker and others, 1986).

METHODOLOGY

Sampling Strategy

The Glarus thrust is magnificently exposed over 15 kilometers from north to south by 21 kilometers from east to west. This configuration allowed for a detailed mapping of the carbon and oxygen isotope pattern in three dimensions as a function of structural setting, metamorphic grade and lithological changes within the footwall. Regional trends are well constrained by more than 30 sampling sites chosen along the thrust (fig. 3). The location of individual sites has been determined according to a regular grid of 5 kilometer spacing. The final distribution is irregular, however, depending on outcrop conditions. At each site, we attempted to characterize the isotope composition ($\delta^{18}O$, $\delta^{13}C$) of calcite of the footwall, the calc-mylonite and the hangingwall. Special emphasis has been placed on the calc-mylonite, and up to 15 hand specimens have been obtained from this very thin horizon at each sampling location. In the case of favorable outcrop conditions, a complete vertical profile across the thrust has been sampled, typically starting 5 meters below the thrust and ending some 10 meters above. Sample intervals were chosen in the decimeter range close to the thrust, metric farther away. Detailed vertical profiles have been acquired for ten sites (fig. 3). Syntectonic veins from within the hangingwall (VF) and the footwall (Tertiary Flysch or Mesozoic carbonates) have been sampled for a comparison of their stable isotope composition with the surrounding matrix.

Analytical Techniques

For the determination of the $\delta^{18}O$ and $\delta^{13}C$ of calcite, 10 to 50 grams of each pre-cleaned rock sample were crushed with a "jaw" crusher to obtain small rock chips (1 to 5 mm), about 10 grams of which were ground again to a homogeneous powder with particle size <40 μm. A tungsten carbide drill bit with a diameter of 3 millimeters was used for the sampling of veins and adjacent matrix. In the case of samples with very small but abundant veins, bulk rock (vein and matrix) and matrix were analyzed separately; the matrix alone was obtained with the drill.

For the determination of $\delta^{18}O$ and $\delta^{13}C$ of calcite, bulk rock powders with an equivalent 0.1 to 0.3 milligrams carbonate content were loaded into individual glass

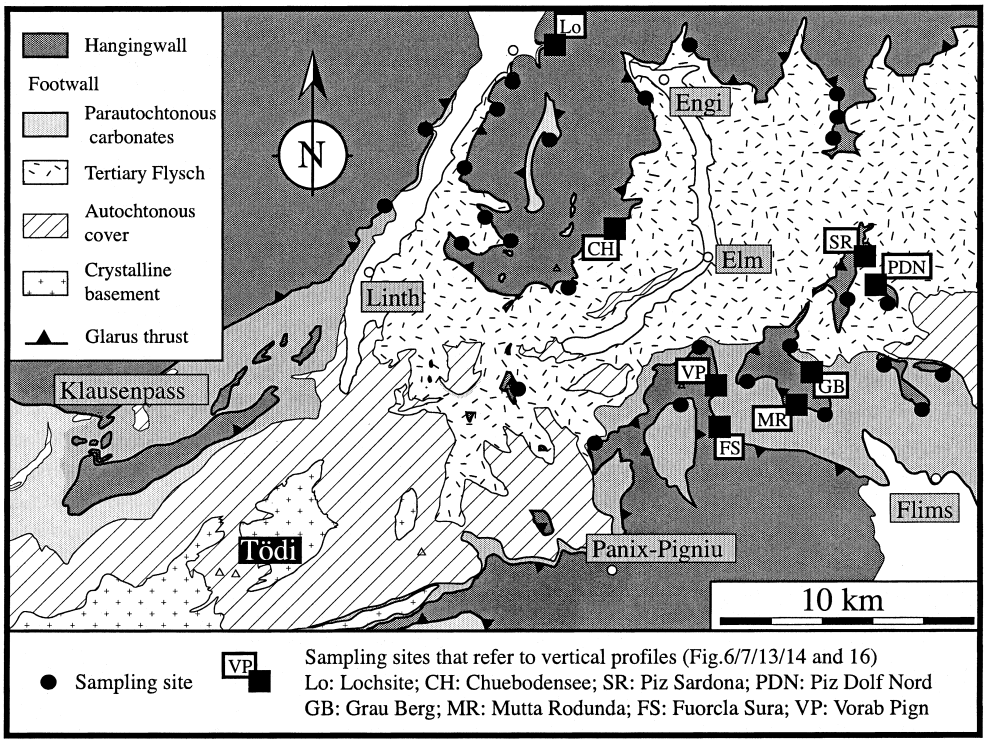

Fig. 3. Simplified tectonic map of the Glarus Alps in eastern Switzerland (modified after Oberholzer, 1933). Sampling sites are indicated together with the sites that refer to figures 6, 7, 13, 14 and 16.

vials. CO_2 was extracted by reaction with 102 percent H_3PO_4 at 70°C for four minutes on a Finnigan Kiel II device. The CO_2 was analyzed on line with a Finnigan-MAT Delta^{plus} isotope ratio mass spectrometer. Reproducibility of replicate measurements was better than 0.1 permil (1σ) for both $\delta^{18}O$ and $\delta^{13}C$.

In addition to bulk rock samples, we analyzed carbonate micro-samples from selected hand specimens. The micro-samples were taken with a dentist drill from polished rock surfaces.

Oxygen isotope analyses of silicates were done on a laser fluorination line of the design described by Sharp (1990). Samples of one to two milligrams were reacted in a BrF_5 atmosphere under a slightly defocused 25 W CO_2 laser beam. The liberated oxygen was separated from excess reagent and reaction by-products cryogenically and by means of a 20 centimeter KBr column kept at 120°C. O_2 was collected on a molecular sieve at liquid nitrogen temperatures and finally expanded into the variable volumes of a Finnigan Delta^{plus} isotope ratio mass spectrometer. UWG-2 garnet (Valley and others, 1995) was used as an internal standard. Reproducibility of replicate measurements was better than 0.15 permil (1σ). Oxygen isotope compositions are given in the conventional δ-notation relative to V-SMOW.

Ratios of $^{87}Sr/^{86}Sr$ were determined at the School of Earth Sciences, University of Leeds. Three selected pre-cleaned slabs of calc-mylonite from three different sites along a north-south profile were used for these analyses and 44 aliquots were obtained using a diamond-tipped dental drill. Sample size varied from 2 to 3 milligrams with a spatial resolution of 1.6 millimeters and a hole depth of 50 μm. In order to obtain data

for pure calcite, aliquots were initially treated with 2.5M HCl at room temperature in screw-top Savillex capsules. Sr was isolated using standard ion exchange technique. For mass spectrometry, Sr was loaded using H_3PO_4 on a single Ta filament. It was then analyzed on a fully automated VG-54E multi-collector mass spectrometer. All Sr data were fractionation corrected to $^{88}Sr/^{86}Sr = 0.1194$ and $^{87}Sr/^{86}Sr$ was normalized to NBS – 987 = 0.71022. Because of the young age of thrust activity of 30 to 20 Ma (Hunziker and others, 1986), age corrections of the data for radiogenic Sr are negligible (Burkhard and others, 1992). The total estimated error is ± 0.00003.

The mineralogical composition of Verrucano samples, taken at 100 meters above the thrust at five specific localities along a north-south profile, was obtained by a combination of XRF for major elements and XRD to identify the different mineral phases present in each sample. About 10 grams of rock powder were used for the XRF analyses and transformed in glassy pastilles with Li-borate that have been analyzed on a Philips PW 2400 spectrometer at the Mineralogical and Petrography Institute of the University of Fribourg (Switzerland).

XRD analyses of the whole rock were carried out at the Geological Institute of the University of Neuchâtel. 800 milligrams of the powder were pressed (20 bars) in a powder holder covered with a blotting paper and analyzed by XRD. Semi-quantitative mineralogical rock composition was determined by XRD (SCINTAG XRD 2000 Diffractometer) based on methods described by Ferrero (1965), Ferrero (1966), Klug and Alexander (1974), Kübler (1983), Rolli, (1990).

A normative mineralogical composition was calculated based on the elemental composition obtained by XRF and on the semi-quantitative XRD determination of the following minerals: apatite, titanite, albite, calcite, dolomite, muscovite, Fe-Mg chlorite and quartz.

RESULTS

Large Scale Calcite Oxygen Isotope Variations in the Calc-mylonite

For each sampling site, a mean $\delta^{18}O$ and $\delta^{13}C$ value has been calculated from up to 15 individual samples. In order to document the large-scale oxygen isotope variations, maps of $\delta^{18}O$ have been constructed by plotting the mean $\delta^{18}O$ value for each sampling site against its geographical coordinates (fig. 4). Interpolation between the different sites has been obtained by kriging. $\delta^{18}O$ values, from 22 permil down to 10 permil, are invariably lowered with respect to the supposed marine carbonate protolith value of 25 permil (Burkhard and others, 1992). Two regional trends can be identified on the $\delta^{18}O$ surface (fig. 4). The values increase from 11 permil in the southeastern exposures to 20 permil farther north. A flattening out at about 20 permil is observed north of the Carbonate-Flysch boundary in the footwall. These trends can also be identified on fig. 5. A striking south-north gradient in the southern part and the flattening out of the values in the north are observed. Despite these obvious regional trends, the calc-mylonite oxygen isotope composition is far from homogeneous. Heterogeneities are large in the south, where they reach 8 permil in individual sites, while in northern sites variations never exceed 3 permil.

A region with slightly higher values of up to 22 permil is found in the northwest (fig. 4), where the hangingwall consists of Mesozoic carbonates.

Calcite Oxygen and Carbon Isotope Variations Across the Thrust

Two groups of profiles have been distinguished, those situated south or north of the carbonate-Flysch boundary in the footwall. Vertical $\delta^{18}O$ profiles of southern sites (fig. 6) display very steep gradients within the first meter above the thrust contact. The most altered values of up to 14 permil are observed at the thrust contact. Higher up within the mylonitized hangingwall, calcite $\delta^{18}O$ value rapidly decrease to typical

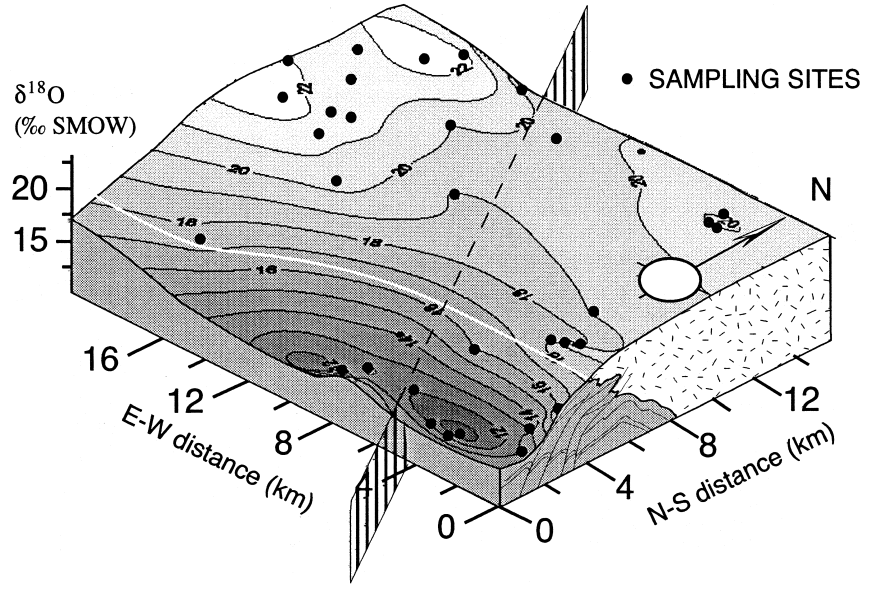

Fig. 4. Regional variations in the mean $\delta^{18}O$ value measured in the Lochsiten calc-mylonite. Horizontal axes are geographic coordinates in km north-south and east-west. Vertical axis is $\delta^{18}O$ (permil-SMOW). Interpolation between sampling sites has been obtained by kriging. The white line represents the carbonate-Flysch boundary in the footwall of the thrust. A schematic cross section of the footwall is indicated on the eastern vertical face of the plot.

unaltered Verrucano values of 10 to 12 permil. In the footwall carbonates, depleted $\delta^{18}O$ values (14 to 22 permil), compared to their expected marine signature of 25 permil, are found up to 7 meters below the thrust contact. They describe a smooth gradient from the contact down into the footwall. Calc-mylonite samples range from 10 to 16 permil.

Carbon isotope compositions of calcite range from 2.3 permil to –5 permil ($\delta^{13}C$ PDB). A very sharp gradient of $\delta^{13}C$ is documented across the thrust contact (fig. 6). Values of calcite in the mylonitized hangingwall show a conspicuous trend of decreasing values from around -2 permil close to the thrust to -5 permil at about 1 meter and higher above the thrust. The width of this alteration zone corresponds quite well to the one observed in $\delta^{18}O$. Uniform marine carbonate $\delta^{13}C$ values (1.3 to 2.6 permil) are found in the footwall limestones, right up to the thrust contact, in contrast with a broad $\delta^{18}O$ alteration zone of several meters wide. Calc-mylonite samples are variably ^{13}C depleted with $\delta^{13}C$ ranging from 2.4 permil to – 4 permil.

Vertical $\delta^{18}O$ profiles of the Verrucano hangingwall of northern sites (fig. 7) are characterized by a broad nearly linear decreasing trend from values around 17 to 19 permil close to the thrust to 10 to 12 permil at 4 meters or higher above the thrust. The distance from the thrust contact to the position where Verrucano background $\delta^{18}O$ composition occurs seems to increase from south to north, from Piz Dolf to Lochsite, where the $\delta^{18}O$ value is still 17 permil at 20 meters above the thrust.

In the footwall Flysch, $\delta^{18}O$ values of calcite of 19 to 20 permil are quite homogeneous independent of the distance below the thrust contact. Calc-mylonite samples are invariably depleted in ^{18}O relative to their presumed marine Helvetic carbonate protolith (25 permil). A clustering of values between 18.5 permil and 20 permil appears in the calc-mylonite of northern sites (fig. 7). This contrasts with a much higher scatter observed in the south (see fig. 6). Carbon isotope composition

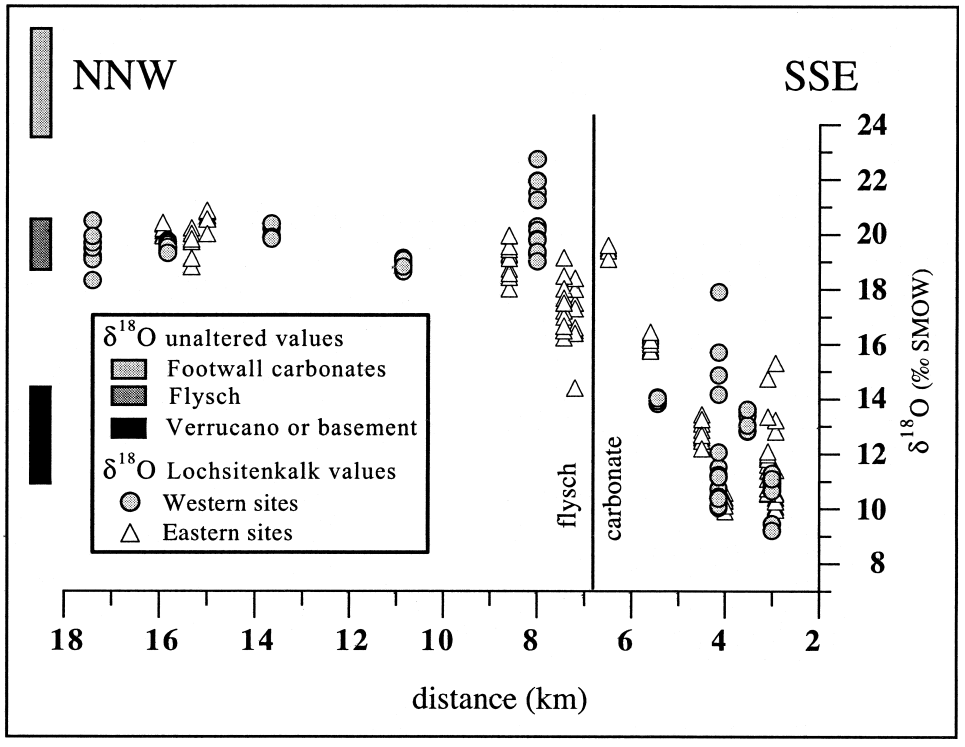

Fig. 5. Plot of calcite $\delta^{18}O$ values of the Lochsitenkalk-mylonite projected onto a NNW-SSE cross section of the Glarus thrust. The range of whole rock isotope composition of the different rock reservoirs is indicated to the left of the $\delta^{18}O$ scale. Two groups of data are distinguished, those from sites situated on the western part of the studied area and those situated in the eastern part (fig. 3) in order to avoid the comparison of sites that are more than 10 km apart from each other. The carbonate-Flysch boundary in the footwall is also indicated.

($\delta^{13}C$) of calcite ranges from 2.3 permil to −6 permil (fig. 7), comparable to that of the southern sites. $\delta^{13}C$ values of calcite in the mylonitized hangingwall show a marked trend of decreasing values from around −2 permil close to the thrust to −6 permil at about 6 meters above the thrust. In the footwall Flysch, the $\delta^{13}C$ values of calcite are quite homogeneous. No trend with respect to distance below the thrust contact could be detected. $\delta^{13}C$ values in the footwall Flysch range from −0.5 permil (at Chuebodensee) to 2 permil (at Lochsite). Within the calc-mylonite, the $\delta^{13}C$ values show little variation and are similar to those of the footwall. In the northern sites, $\delta^{13}C$ and $\delta^{18}O$ vertical profiles display the same features. A smooth gradient prevails in the hangingwall, whereas the $\delta^{13}C$ and $\delta^{18}O$ values are homogeneous in the footwall, independent of the distance to the thrust contact. This correlation of $\delta^{13}C$ and $\delta^{18}O$ vertical profiles in the north strongly contrasts with the southern sites where the $\delta^{13}C$ and $\delta^{18}O$ vertical profiles are completely different.

"Background" Oxygen Isotope Composition of the Verrucano Formation

To constrain potential large-scale $\delta^{18}O$ variations within the Verrucano hangingwall, 6 whole-rock samples from 5 sites along a south-north profile were examined. The "normative" mineralogical composition and the $\delta^{18}O$ of calcite and of the bulk rock have been determined. No regional trend in $\delta^{18}O$ could be detected (fig. 8). $\delta^{18}O$ values are fairly homogeneous, about 13 permil for calcite and about 12 permil for the

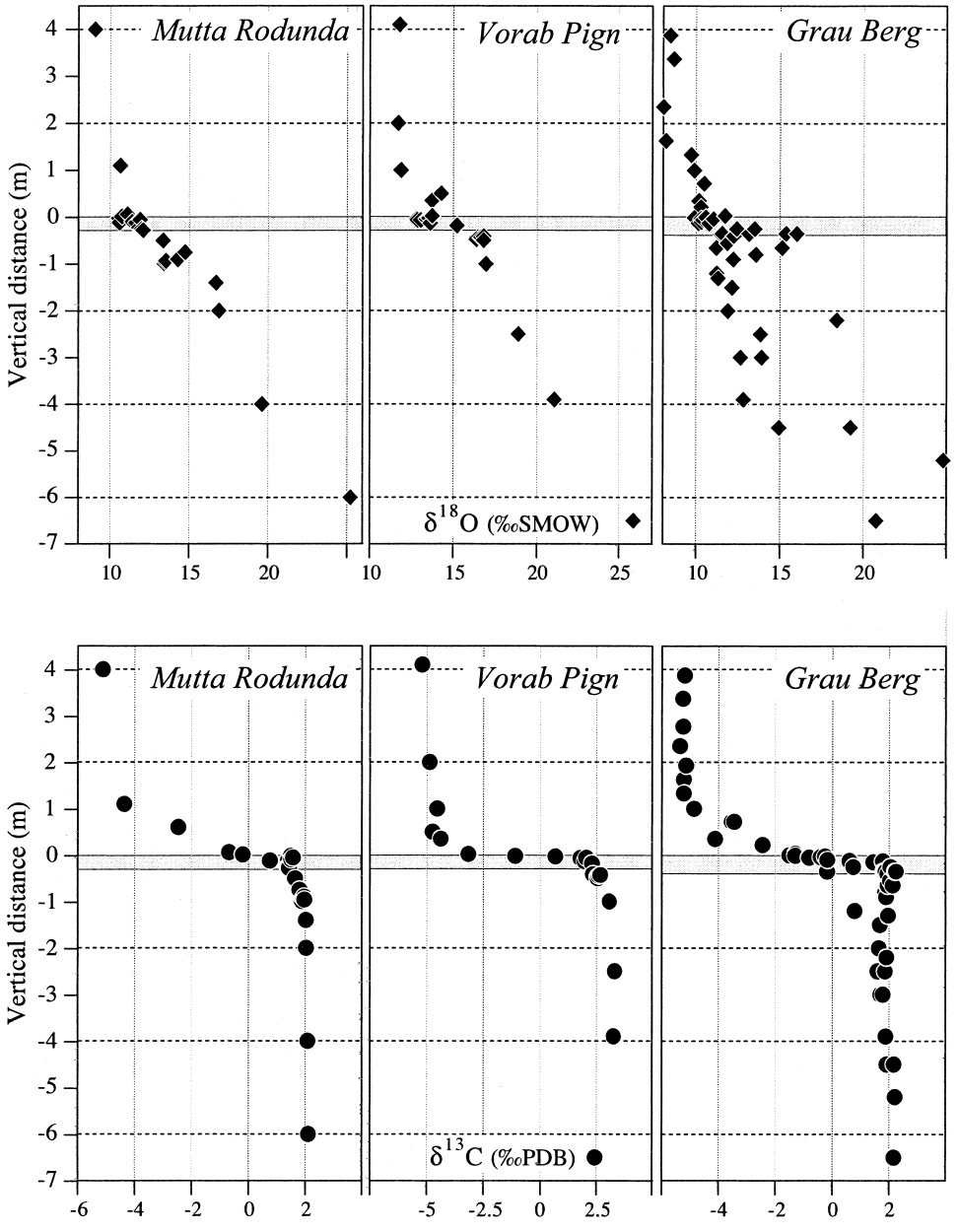

Fig. 6. $\delta^{18}O$ and $\delta^{13}C$ values of calcite versus vertical distance across the Glarus thrust from three localities in the southern part of the study area (fig. 3). The gray shaded area represents the Lochsiten calc-mylonite at the thrust contact. The hangingwall consists of Permian Verrucano siltstones, the footwall of Mesozoic carbonates.

bulk rock. One exception is present at Kärpf, with a mean $\delta^{18}O$ value of 15.5 permil for calcite and about 14.5 permil for the bulk rock. In addition, the $\delta^{18}O$ of quartz in equilibrium with the whole rock was calculated for each sample (fig. 8), based on the normative mineralogy, an assumed temperature of 300°C and standard isotopic

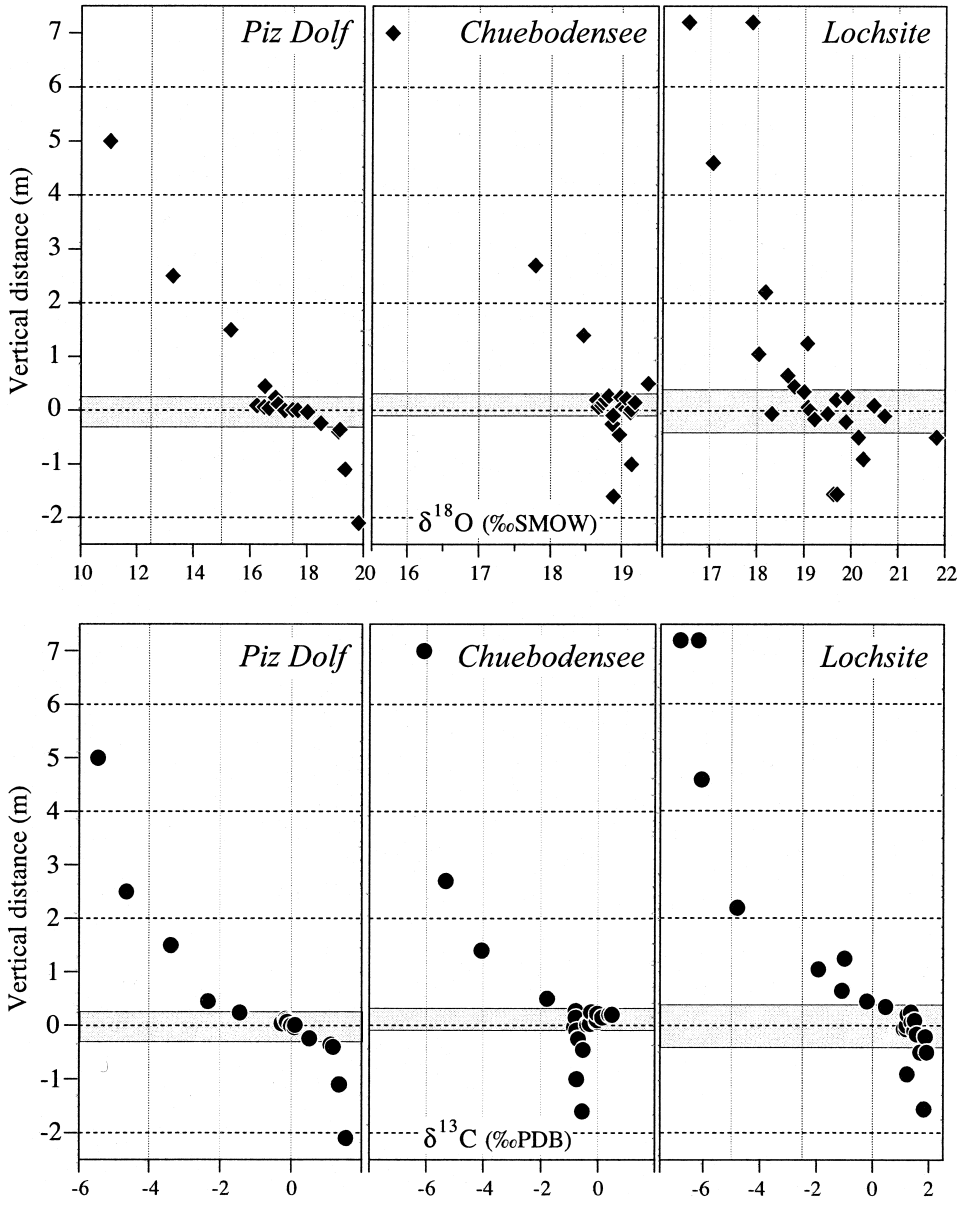

Fig. 7. $\delta^{18}O$ and $\delta^{13}C$ values of calcite versus vertical distance across the Glarus thrust from three localities in the northern part of the study area (fig. 3). The gray shaded area represents the Lochsiten calc-mylonite at the thrust contact. The hangingwall consists of Permian Verrucano siltstones, the footwall of Tertiary Flysch. The 0 reference on the vertical scale corresponds to the septum, a planar horizon that crosscut all internal structures of the calc-mylonite.

fractionation factors (Clayton, Goldsmith, and Mayeda, 1989; O'Neil, Clayton, and Mayeda, 1969). Mineralogically, a systematic trend of increasing quartz and muscovite content towards the north at the expense of chlorite is documented. This trend is reflected in the calculated $\delta^{18}O$ composition of quartz, decreasing slightly from 16

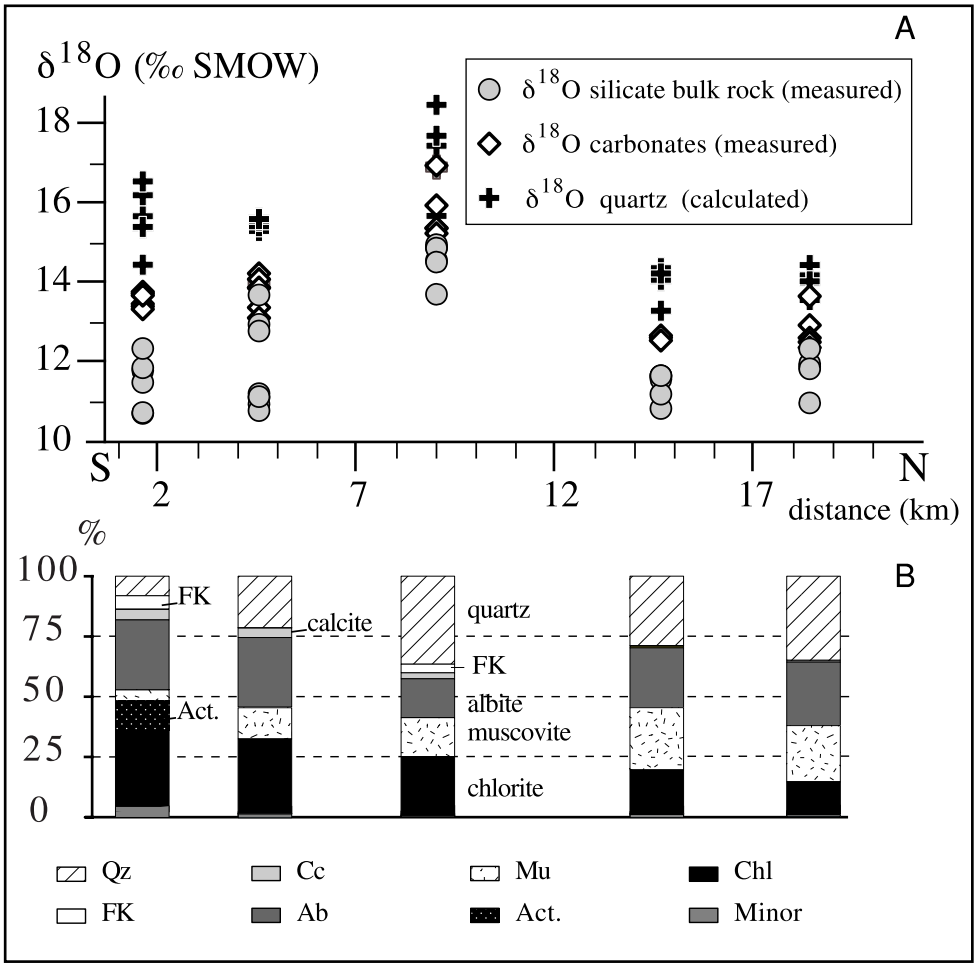

Fig. 8. A) $\delta^{18}O$ values of calcite, bulk rock and calculated quartz in equilibrium with Verrucano samples from five sites situated 100 m above the thrust versus north-south distance along the Glarus thrust (upper part). B) Mineralogical composition of the Verrucano samples as calculated by an adapted norm based on XRF and XRD data.

permil ±1 to 15 permil ±1. However, with one out of the 5 sampling sites being an outlier (17 permil ±1), this trend is hardly significant.

$\delta^{18}O$ and $\delta^{13}C$ Co-variation of Calcite from Footwall and Hangingwall Veins and Matrix

In samples of footwall and hangingwall with macroscopic veins (fig. 9) they invariably have $\delta^{18}O$ and $\delta^{13}C$ values close to their matrix or bulk rock. The largest differences observed between vein and wall rock are 2 permil for $\delta^{18}O$ and 0.5 permil for $\delta^{13}C$. While Flysch samples are clustered, between 20 and 22 permil in $\delta^{18}O$, both hangingwall Verrucano and footwall carbonate samples have a large spread of values. Calcites from the mylonitized Verrucano show large variations both in $\delta^{18}O$ (12 to 21 permil) and $\delta^{13}C$ (−6 to 1.5 permil). The highest values are strongly enriched compared to unaltered original Verrucano values (12 permil in $\delta^{18}O$ and −6 permil in $\delta^{13}C$). Calcites from footwall carbonates display a large range of depleted values in $\delta^{18}O$ (15 to 21%) but are relatively homogeneous in $\delta^{13}C$.

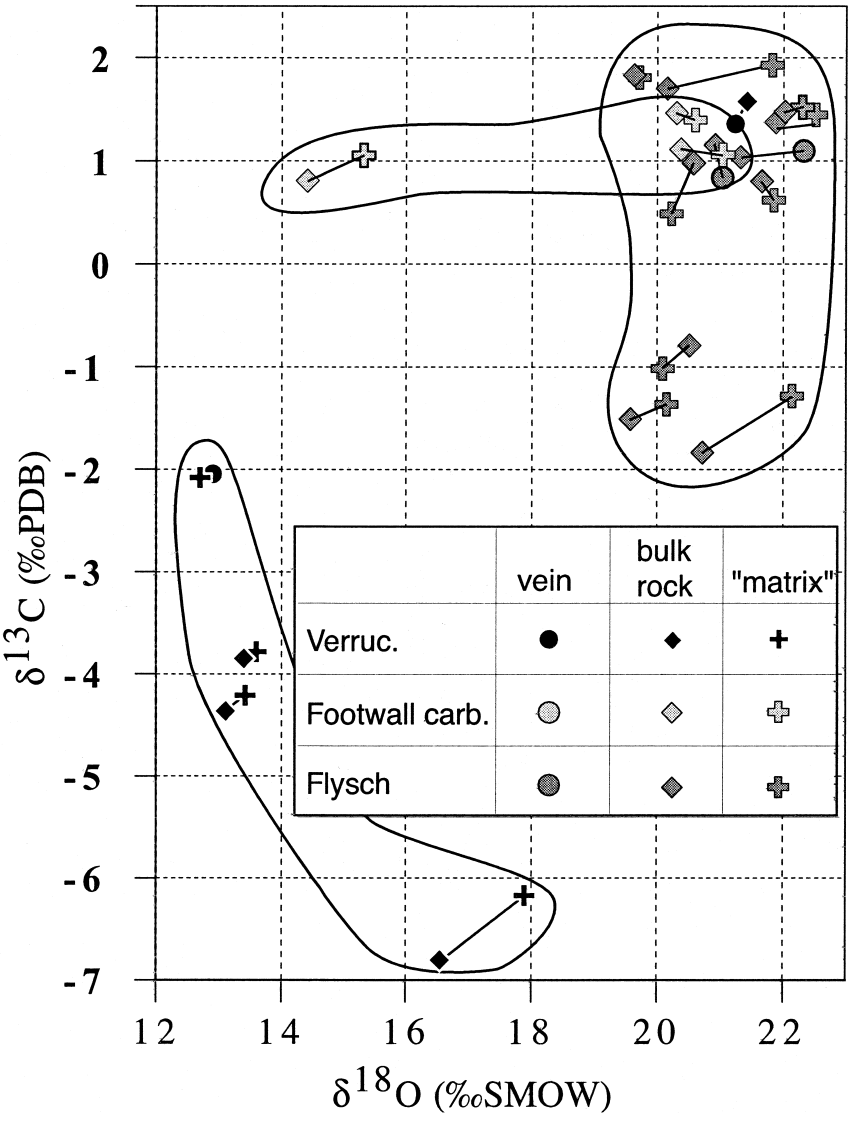

Fig. 9. Comparison of calcite veins and their immediate wall-rock matrix, represented in $\delta^{18}O$ vs. $\delta^{13}C$. VF, footwall carbonates and Flysch samples from different sites along the Glarus thrust are distinguished by different symbols. A clear clustering appears for the Flysch calcites, whereas footwall carbonates and Verrucano calcites display large degrees of heterogeneity.

$^{87}Sr/^{86}Sr$ of the Calc-mylonite

$^{87}Sr/^{86}Sr$ has been analyzed on three slabs of calc-mylonite from three different southern sites: Fuorcla Sura, Vorab Pign and Sardona from south to north (fig. 3). The top of each slab corresponds to the calc-mylonite Verrucano contact (fig. 10). Vertical $^{87}Sr/^{86}Sr$ profiles are characterized by a zone of homogeneous values at the top with a thickness of less than 4 centimeters in Fuorcla Sura and Vorab Pign and of at least 13 centimeters in Sardona (fig. 10). The mean $^{87}Sr/^{86}Sr$ value in this zone decreases from Fuorcla Sura (0.7125) to Vorab Pign (0.7110) and to Sardona (0.7104). Petrographi-

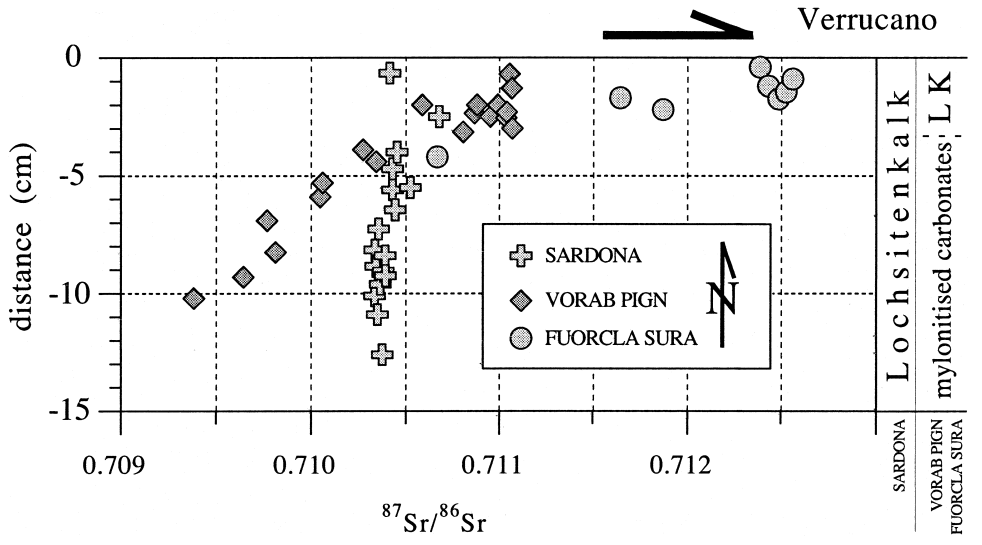

Fig. 10. $^{87}Sr/^{86}Sr$ values of calc-mylonite calcite versus vertical distance across the Glarus thrust (fig. 3). The footwall consists of mylonitized carbonates in Fuorcla Sura and Vorab Pign, of Flysch in Sardona. Note the different thickness of the Lochsiten calc-mylonite between Sardona and the two other localities.

cally, this zone of homogeneous $^{87}Sr/^{86}Sr$ values corresponds to a sub-millimeter-sized alternation of white/yellow layers and dark stylolitic seams. The light layers are easily recognized as strongly deformed veins. This zone corresponds to the true calc-mylonite known as Lochsitenkalk. In the two slabs from Fuorcla Sura and Vorab Pign, $^{87}Sr/^{86}Sr$ values follow a decreasing trend towards a typical marine carbonate signature of 0.708. Petrographically, these trends have been identified within gray mylonitized footwall carbonates with very little veiny material. At Sardona, no decreasing trend was observed. Veiny Lochsitenkalk mylonite is 2 meters thick here and no mylonitized Mesozoic carbonate has been identified. Moreover, the alternation of white/yellow layers and dark stylolitic seams is intensively folded and disrupted.

DISCUSSION

Regional $\delta^{18}O$ Trends of the Calc-mylonite

The non linear regional trend of increasing $\delta^{18}O$ values of the calc-mylonite from 11 permil in the southernmost exposures to 17 to 19 permil slightly north of the lithological boundary between Cretaceous limestones and Tertiary Flysch in the footwall of the thrust (figs. 4, 5) has been interpreted as an oxygen isotope front (Bowman, Willett, and Cook, 1994; Burkhard and others, 1992). A possible scenario to explain the observed pattern is migration of ^{18}O depleted, externally-derived fluids in a pre-existing limestone or calc-mylonite along the thrust. The oxygen isotope signature of the presumed marine Helvetic carbonate protolith should be around 25 permil (Burkhard and others, 1992). A $\delta^{18}O$ of 6 permil for the infiltrating fluid is inferred from the observation of $\delta^{18}O$ values as low as 11.5 permil in the southernmost exposures of the calc-mylonite and a calculated oxygen isotope fractionation of 5.5 permil for H_2O-calcite at 300° according to O'Neil, Clayton, and Mayeda (1969). Such fluids could be derived either from the overlying Verrucano or from dehydration of the Infrahelvetic Basement during prograde metamorphism in the footwall and root zone of the thrust. We favor the latter solution; a Verrucano origin is rejected because

there is no reason why and how a north-south front should have developed above marine carbonates found in the footwall of the southern Glarus thrust. Furthermore, the Verrucano hangingwall is considered as an unlikely fluid source during thrusting deformation which at least partly post-dates metamorphism in this formation. Farther north, however, where Verrucano is overriding Tertiary Flysch series, the calc-mylonite clearly interacted with fluids derived from the adjacent footwall.

As predicted by transport theory (see Baumgartner and Rumble, 1988; Bickle and McKenzie, 1987), an original step-like isotopic front will be displaced by advective fluid transport in the direction of flow by a distance proportional to the total flux. Coupled advective and diffusive/dispersive transport will result in displacement and broadening[1] of the front. Dispersion is the process of mixing that is due to the heterogeneity of velocities caused by tortuosity in the porous medium.

Assuming equilibrium exchange, the position of the front with respect to the supposed fluid inlet bears information on the time integrated fluid flux (TIFF) along the thrust. The shape of the front, in particular its distension with regard to a supposed initially sharp front, contains information on the amount of diffusive/dispersive contributions to material transport. In advective diffusive/dispersive transport, an initially sharp front is broadened symmetrically around the advectively displaced position of the initial front. The diffusive/dispersive broadening of an initially sharp front between two different fluid reservoirs is governed by (Crank, 1975):

$$R(x, t) = R_f + 0.5(R_f - R_r) * \operatorname{erfc} \frac{x + \omega}{2\sqrt{u}} \qquad (1)$$

where R_f is the composition in equilibrium with the infiltrating fluid, R_r is the composition in equilibirum with the protolith, $u = D*t$ and u is referred to as the characteristic length of dispersion/diffusion, t is time and D is the effective dispersion/diffusion coefficient. The parameter ω, $\omega = \upsilon*t$, gives the advective displacement of the front with respect to its original position, where υ is the mean interstitial particle velocity.

The parameters u and ω may be obtained from fitting the function R(x,t) to the observed data south of the carbonate-Flysch boundary in the footwall by non linear least square minimization (fig. 11). This procedure yields a D*t of 2.3 and 0.38 km for the western and eastern cross section, respectively, and advective front displacements ω of 5.9 and 3 kilometers for the western and eastern cross sections, respectively (fig. 11).

There is no rigorous way to extract either time t, D or υ from this result. However, if either one is specified, the others are fixed by the front geometry. If oxygen dispersivities/diffusivities are calculated for geologically meaningful time scales, then effective oxygen dispersivities/diffusivities on the order of 10^{-12} to 10^{-10} m^2/s are obtained (see table 1). It must be underlined that these are effective dispersivities/diffusivities. The effective dispersion/diffusion coefficient of a species in the pore fluid

[1] Distension of sharp fronts may also occur if the rate of fluid-rock reaction is slow compared to fluid infiltration velocities (Abart, R., and Pozzorini, D., 2000; Abart, R., and Sperb, R., 1997; Bowman, J. R., Willett, S. D., and Cook, S. J., 1994; Lassey, K. R., and Blattner, P., 1988).The Damköhler number N_D is defined as:

$$N_D = \frac{k_k \phi L}{q} \qquad \text{(Bowman, J. R., Willett, S. D., and Cook, S. J., 1994)}$$

where q is the volumetric fluid flux, L is a scaling distance, ϕ is the porosity and k_k is the reverse rate of isotopic exchange. q/ϕ is known as the mean interstitial particle velocity υ . N_D relates the rates of advective transport and mineral-fluid exchange. High Damköhler numbers stands for scenarios with relatively rapid isotopic exchange rates, that is, close to local equilibrium exchange.

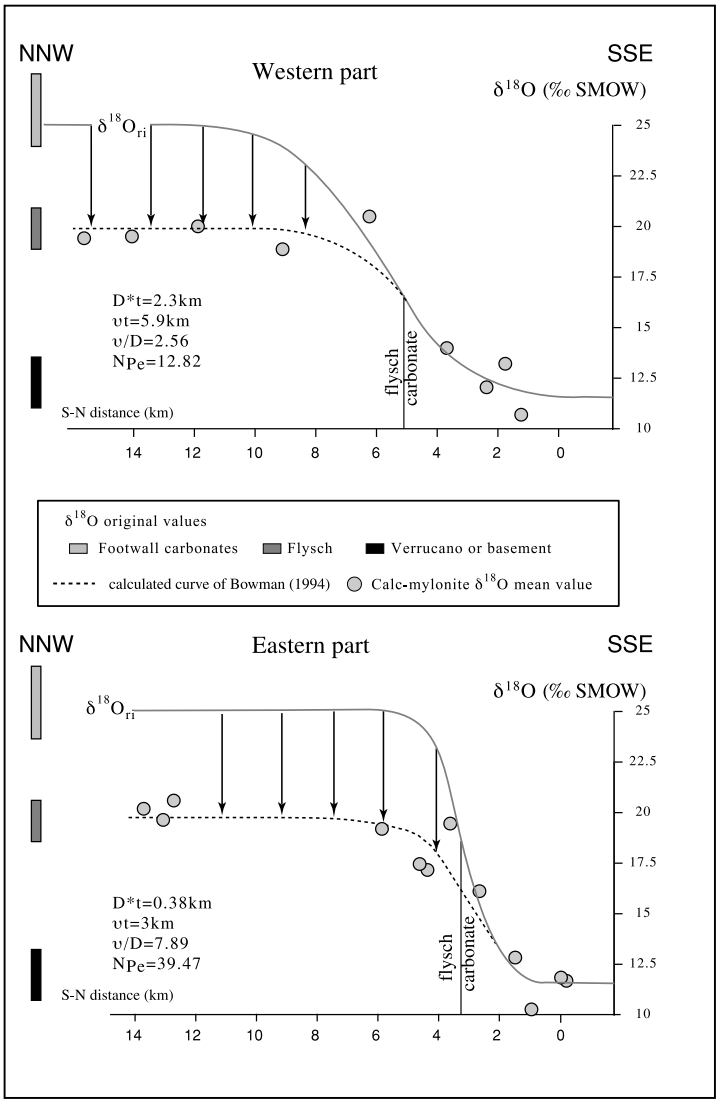

Fig. 11. Calculated curves for calcite $\delta^{18}O$ composition against north-south distance predicted by transport theory applied to the infiltration of a fluid with an $\delta^{18}O$ of 6 permil into a pre-existing carbonate with an original $\delta^{18}O$ of 25 permil. These curves are represented together with the data point of mean $\delta^{18}O$ of the calc-mylonite at each site. Only those sites where footwall is represented by carbonates were considered to fit the curves with the data. A western and an eastern cross-section have been distinguished to avoid comparison of sites that are more than 10 km apart. N_{Pe}, the Pecklet number, expresses the relative contribution of advective to diffusive/dispersive transport mechanisms. t is time and D is the effective oxygen dispersion/diffusion coefficient. D*t is referred to as the characteristic length of dispersion/diffusion. υ*t, gives the advective displacement of the front with respect to its original position, where υ is the mean interstitial particle velocity.

of a porous medium, D, is related to the diffusivity of the same species in the free fluid, D_0, by:

$$D = \tau \times \phi \times D_0 \qquad \text{(Abart and Pozzorini, 2000)} \qquad (2)$$

TABLE 1

Fluid flow parameters along north-south profiles

t (years)	t (s)	D (m^2/s)	υ_{east} (m/s)	υ_{west} (m/s)
10^5	$3.15X10^{12}$	$7.3X10^{-7}$	$1.4X10^{-9}$	$1.9X10^{-10}$
LE 10^6	$3.15X10^{13}$	$7.3X10^{-8}$	$1.4X10^{-10}$	$1.9X10^{-11}$
10^7	$3.15X10^{14}$	$7.3X10^{-9}$	$1.4X10^{-11}$	$1.9X10^{-10}$

Fluid flow parameters deduced from fitting curves with $\delta^{18}O$ data of calc-mylonite along two north-south profiles. The calculation is based on transport theory. t is time, D is the dispersive/diffusive coefficient and υ is the mean interstitial particle velocity for the channelized flow system that occurred in the southern part of the Glarus overthrust. A western and an eastern cross-section have been distinguished to avoid comparison of sites that are more than 10 km far from each other.

where τ is the tortuosity and ϕ is the porosity of the porous medium. The diffusivity of the H_2O species in water is about $5 \cdot 10^{-8}$ m^2/s at 300°C (experimental data compiled by Franck and others, 1996). The porosity in geologic materials may vary considerably, whereas tortuosity may only vary between <1 and 0.1.

If ϕ were 10^{-2} and τ were 0.1, an effective dispersivity/diffusivity of $5 \cdot 10^{-11}$ m^2/s, and if ϕ were 10^{-3} and τ were 0.1, an effective dispersivity/diffusivity of $5 \cdot 10^{-12}$ m^2/s would be calculated from the experimental data. This is at least two orders of magnitude slower than the phenomenological oxygen diffusivities/dispersivities obtained for geologically relevant time scales from the geometry of the $\delta^{18}O$ front along the Glarus thrust. Hydrodynamic dispersion in the course of flow along the thrust may be responsible for the enhancement of oxygen diffusion/dispersion.

If the distance of displacement of the front ω (υ*t) is known, the total flux can be calculated. In the case of the Glarus thrust, the initial position of the front is uncertain, because the root zone of the thrust is not exposed and the geometry of the different lithological units and potential fluid sources in the root zone are not known. One may, however, obtain a minimum estimate of the time-integrated fluid flux (TIFF), if the northernmost conceivable position of the fluid inlet is considered. Bowman and others (1994) placed the fluid inlet at Grauberg (compare with fig 11). We shift the position of the fluid inlet farther south to a position where the mean $\delta^{18}O$ values of all model fronts coincide with the presumed fluid buffered composition of the calc-mylonite to within 0.1 permil.

The inferred front displacements, ω (υ*t), are 5.9 and 3 kilometers for the western and eastern cross-sections respectively. The time integrated fluid flux is related to front displacement by:

$$TIFF = \omega \times K_d \tag{3}$$

where Kd, known as the solid/fluid partition coefficient, expresses the partitioning of oxygen between equivalent volumes of rock and pore fluid. Kd is given by:

$$Kd = \frac{nO_{rock} \cdot V_{fluid}}{nO_{fluid} \cdot V_{rock}} \tag{4}$$

where nO_{rock} and nO_{fluid} give the number of moles of oxygen per mole of rock and fluid, respectively, and V_{fluid} and V_{rock} refer to the molar volumes of fluid and rock. Considering the calc-mylonite as pure calcite and the fluid as pure water at 300°C and 3

to 4.5 kbar results in V_{rock} = 37 cm^3/mol and V_{fluid} = 19 cm^3/mol, and Kd = 1.5. This yields TIFF of 4500 m^3/m^2 and 9100 m^3/m^2 (compare Bowman, Willett, and Cook, 1994) for the eastern and western cross sections, respectively. From a comparison of the characteristic length of diffusion (D*t) and the displacement ω (υ*t) of the front with respect to its presumed initial position, the relative contributions of advection and diffusion/dispersion may be estimated (N_{Pe} = υL/D).[2] The υ/D ratios for the eastern and western cross-sections are 7.89 and 2.56. If this is multiplied with an arbitrarily defined scaling length L = 5 km (compare Bowman, Willett, and Cook, 1994), Pecklet numbers $N_{Pe}^{(1)}$ of 39.47 and 12.82 result for the eastern and western profiles, respectively (fig. 11) and indicate a very important role of dispersion/diffusion (compare Bowman, Willett, and Cook, 1994).

It must be stated that the above model is strictly one-dimensional and therefore does not consider the influence of footwall or hangingwall on the isotopic signature of the calc-mylonite. The isotopic alteration of the uppermost five meters of the footwall carbonates and the lowermost 1 meter of the hangingwall indicates that the infiltrating fluid also exchanged its oxygen with the isotopically heavy footwall as well as, to a lesser extent, with the isotopically relatively light hangingwall. This scenario may be envisioned as a loss of tracer into the country rocks of a thrust parallel fluid conduit. The net effect of such transversal tracer loss is to increase the retardation of the oxygen front with respect to the strictly one dimensional scenario. The inferences made from the 1-D model must therefore be considered as minimum estimates of both integrated fluxes and characteristic length scales of diffusion.

Towards the north, the O-isotope front measured within the calc-mylonite deviates significantly from an ideal symmetric shape predicted by transport theory for flow along the thrust in a pre-existing carbonate with an initial $\delta^{18}O$ marine signature of 25 permil (fig. 11). The front rapidly flattens at about 20 permil. In the interpretation of Bowman, Willett, and Cook (1994), this segment corresponds to the downstream part of the isotope front where no alteration of the pre-existing carbonate has occurred. This anomaly is best explained as an influence of the underlying Flysch however (see fig. 4). Northward, the calc-mylonite O-isotope composition rapidly converges toward the Flysch oxygen isotope composition rather than toward a marine Mesozoic carbonate signature (fig. 11). We think that most of the calc-mylonite in the northern part formed by precipitation of veins from fluids expelled from the underlying Flysch (see below). This interpretation also explains the weak dispersion of $\delta^{18}O$ values in the north. In the southern part, the marked heterogeneity reflects contrasting calcite $\delta^{18}O$ signatures resulting from a mixture of variably altered marine carbonates and secondary calcite precipitated from an external ^{18}O-depleted fluid (see Bowman, Willett, and Cook, 1994).

In the northwestern part of the study area, Mesozoic marine carbonates are found in the hangingwall thrust over Flysch in the footwall. Here the calc-mylonite at least partly consists of highly sheared carbonates derived from the hangingwall. which have interacted with slightly ^{18}O-depleted fluids coming from the Flysch below. Accordingly, calcite $\delta^{18}O$ values in the calc-mylonite are up to 22 permil.

[2] The Peclet number (N_{Pe}) is defined as: $N_{Pe} = \frac{qL}{\phi D}$ for example, Bickle, M. J., and Baker, A. J. (1990). where and D is the dispersion/diffusion coefficient. The Pecklet number expresses the relative contribution of advective to diffusive/dispersive transport mechanisms (Bickle, M. J., and Baker, A. J., 1990). High Peclet numbers (∞) stands for advection-dominated transport.

Calcite $\delta^{18}O$ and $\delta^{13}C$ Vertical Profiles Across the Thrust

The isotopically contrasting footwall and hangingwall lithologies may be regarded as two distinct carbon and oxygen reservoirs, which exchanged material by diffusive/dispersive and advective transport. In the south, where the main flow component most likely was thrust parallel, consideration of the vertical isotope variation within the framework of 1-D models in the direction perpendicular to the thrust may be employed to investigate cross thrust transport components (see also Abart and others, 2002). The trend of increasing $\delta^{18}O$ values from 11-15 permil at the thrust contact to 24 permil 7 meters below (fig. 6) is interpreted as an isotope front, which developed by isotopic exchange of the footwall carbonates with a relatively ^{18}O depleted reservoir. From the Verrucano/calc-mylonite contact down into the footwall, the calcite $\delta^{13}C$ values describe a very sharp increasing trend (fig. 6). This exchange front is significantly retarded with respect to the oxygen isotope front. In the hangingwall, very sharp $\delta^{18}O$ and $\delta^{13}C$ gradients are described (fig. 6). Only the first 50 to 100 centimeters display $\delta^{18}O$ and $\delta^{13}C$ values resulting from the interaction between the Verrucano and a relatively ^{18}O and ^{13}C enriched fluid.

One possibility to model the exchanges that occurred by combined dispersive/diffusive-advective transport at the thrust contact (fig. 12, left) is to regard the

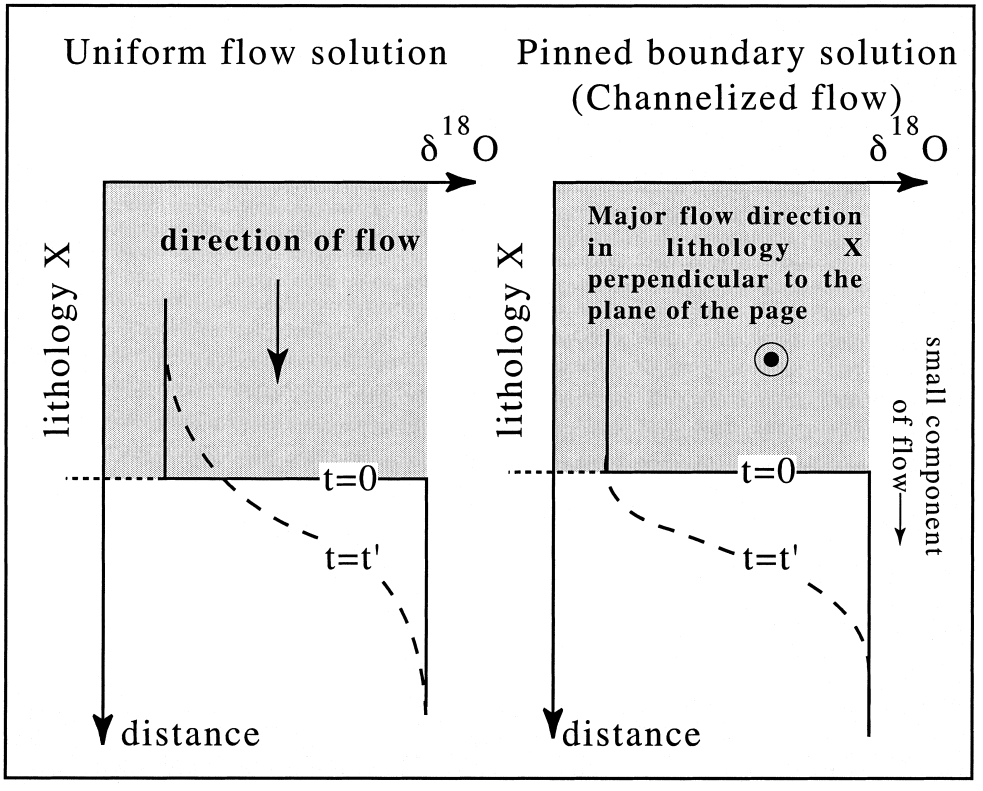

Fig. 12. Diagrammatic illustration of transport isotope step for different boundary conditions. On the left, the uniform flow advection displaces step and diffusion/dispersion smoothes this step. On the right, the pinned boundary solution indicates that copious flow in the lithology X, mainly parallel to layering, maintains the isotopic composition at the boundary at a constant value. Both diffusion/dispersion and a smaller component of flow transport this isotopic composition into the lower layer (modified after Bickle and Baker, 1990)

transport parameters, that is, fluid flow velocity and effective oxygen diffusivity as constants across the thrust (homogeneous flow model, according to Bickle and Baker, 1990). In this case the isotope composition is given by equation (1).

The corresponding model curves fitted to our data are shown in figure 13. The characteristic diffusion lengths are 3, 3, and 6.8 meters for the Mutta Rodunda, Vorab Pign, and Grauberg localities. The corresponding advective front displacements are 2.3, 2.3, and 3.8 meters downwards from the thrust. Considering the footwall carbonates as pure calcite and the fluid as pure water at 300°C and 3 to 4.5 kbar results in Kd = 1.5 (see above). This yields TIFF of 3.45, 3.45 and 5.7 m^3/m^2 for Mutta Rodunda, Vorab Pign and Grauberg respectively for the downward infiltration of fluids into the footwall. This is three orders of magnitude lower than the calculated TIFF of flow along the thrust. The characteristic diffusion length and advective front displacements obtained for carbon is significantly smaller (see fig. 13). The strong retardation of the carbon, with respect to the oxygen fronts testifies to a very low carbon to oxygen ratio in the fluid on the order of 1/1000 to 1/100.

Considering the relatively minute isotopic effects in the hangingwall and the pronounced alteration halo below the thrust (fig. 12, right), one may, alternatively, regard the hangingwall as an infinite reservoir, which buffers the oxygen and carbon isotope compositions at the thrust contact (pinned boundary model according to Bickle and Baker, 1990). If downward transport is then regarded as a diffusive/dispersive process, the isotope composition is given by (Crank, 1975):

$$R(x, t) = R_r - (R_f - R_r) * \operatorname{erfc} \frac{x + \omega}{2\sqrt{u}} \qquad (5)$$

The corresponding model curves fitted to our data are shown in fig. 14. In this model, the entire transport is attributed to diffusion/dispersion. Accordingly, the inferred diffusion length of 3.2, 3.2, and 8.3 respectively, are larger than in the homogenous flow model. As in the previous model, the strong retardation of the carbon, with respect to the oxygen fronts testifies to low C/O ratios in the pore fluid. In figure 15A, the data from the calcites of the footwall carbonates describe an L-shaped pattern that testify to interaction with ^{18}O, ^{13}C depleted fluid ($\delta^{18}O$ = 6 to 8 permil and $\delta^{13}C = -7$ permil) that had a very low X_{CO2} (Bickle and McKenzie, 1987). Oxygen diffusivities derived from the characteristic diffusion length and retarded flow velocities for geologically relevant time scales are given in table 2. These are well within the range of oxygen diffusivities that would be predicted for porous rocks from experimental data on the self-diffusion of H_2O in water.

In summary, modeling indicates that cross thrust transport is several orders of magnitude slower than thrust parallel transport inferred from the south-north oxygen isotope front as attested by the differences in TIFF. Cross thrust fluid transport is significant, however, and preferentially in the downward direction leaving their imprint on the uppermost few meters of the footwall carbonates.

Hydrodynamic dispersion on either side of the thrust contact is the most plausible explanation for the observed alteration in the hangingwall. Fluids flowing along the thrust penetrate the footwall and hangingwall by hydrodynamic dispersion. If a fluid has traveled through the footwall and has been enriched in ^{18}O and ^{13}C before infiltrating the hangingwall, a slight enrichment of the Verrucano will result. Details of these processes are discussed in Abart and others (2002).

In the northern area, decreasing trends of calcite $\delta^{18}O$ and $\delta^{13}C$ values have been identified from the thrust up into the hangingwall (fig. 7), whereas footwall and calc-mylonite are indistinguishable in $\delta^{18}O$ and $\delta^{13}C$. No sign of downward infiltration of fluids can be detected in the footwall. These observations are best explained by Flysch-derived fluids infiltrating upward into the VF. The calc-mylonite itself is ex-

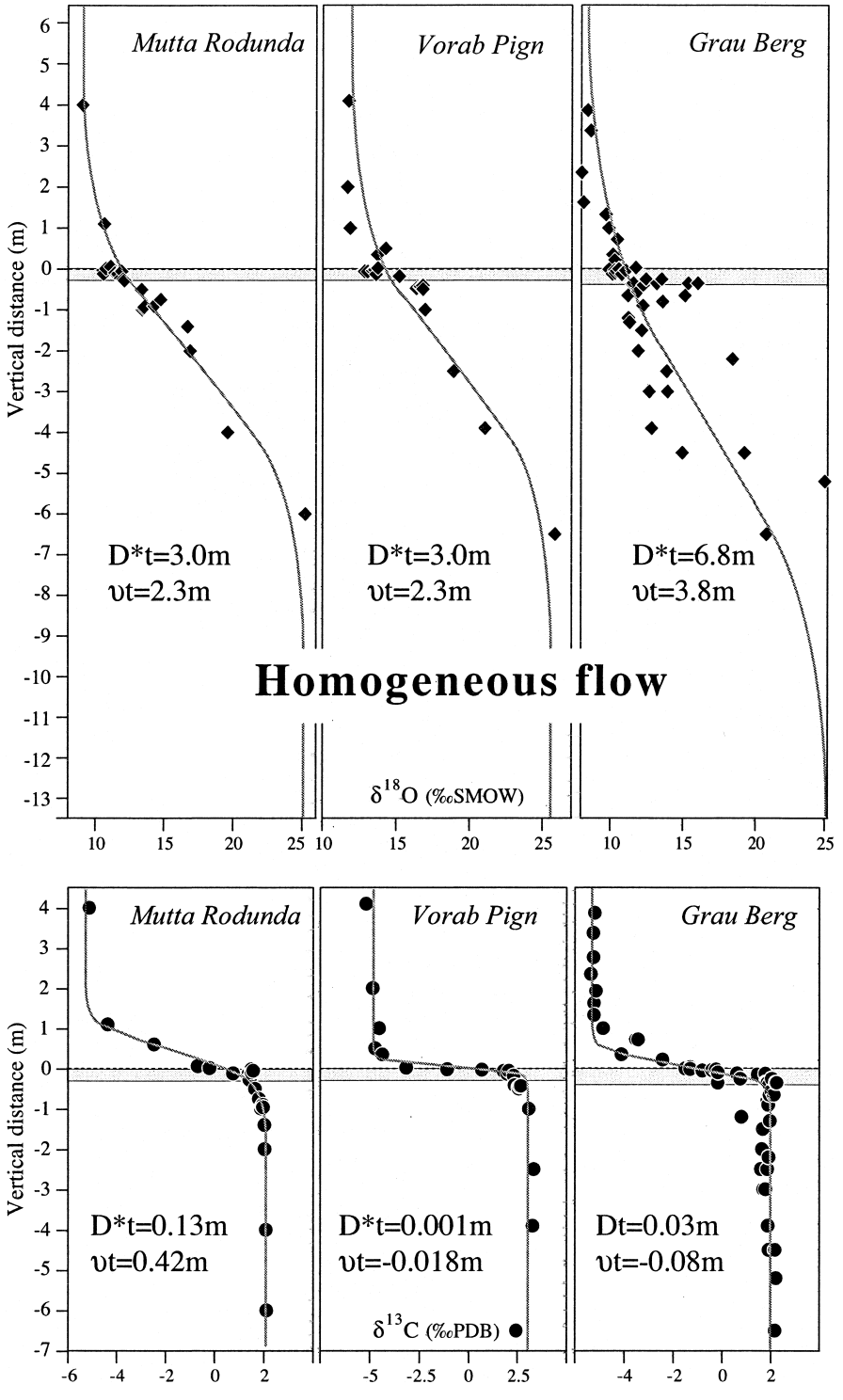

Fig. 13. Calculated curves for calcite $\delta^{18}O$ (upper part) and $\delta^{13}C$ (lower part) composition against vertical distance predicted by homogeneous flow model of Bickle and Baker (1990) are represented together with the $\delta^{18}O$ and $\delta^{13}C$ data from three sites of the southern part of the Glarus overthrust. t is time and D is the effective oxygen dispersion/diffusion coefficient. D*t is referred to as the characteristic length of dispersion/diffusion. υ*t, gives the advective displacement of the front with respect to its original position.

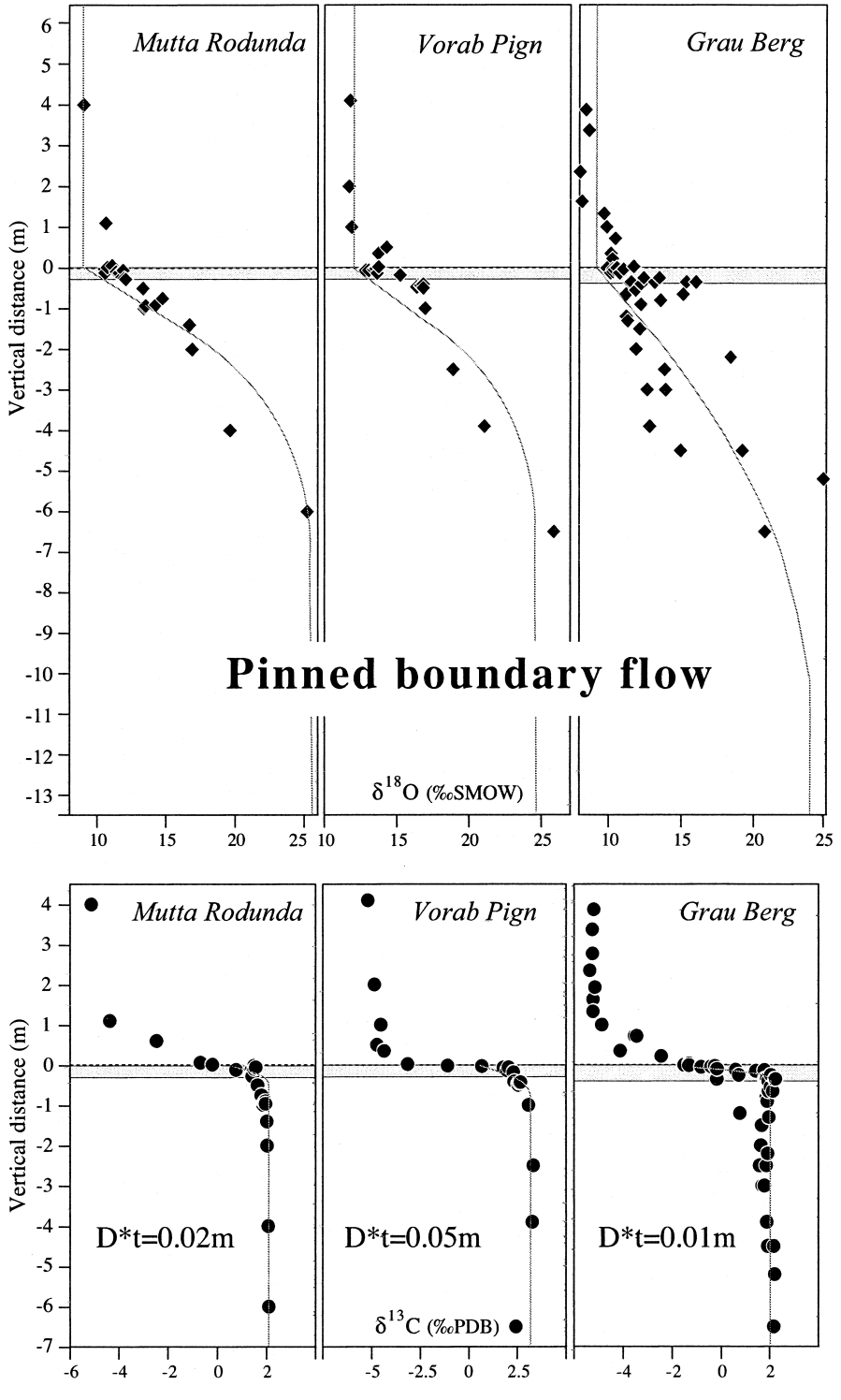

Fig. 14. Calculated curves for calcite $\delta^{18}O$ (upper part) and $\delta^{13}C$ (lower part) composition against vertical distance predicted by pinned boundary flow model of Bickle and Baker (1990) are represented together with the $\delta^{18}O$ and $\delta^{13}C$ data from three sites of the southern part of the Glarus overthrust. t is time and D is the effective oxygen dispersion/diffusion coefficient. D*t is referred to as the characteristic length of dispersion/diffusion.

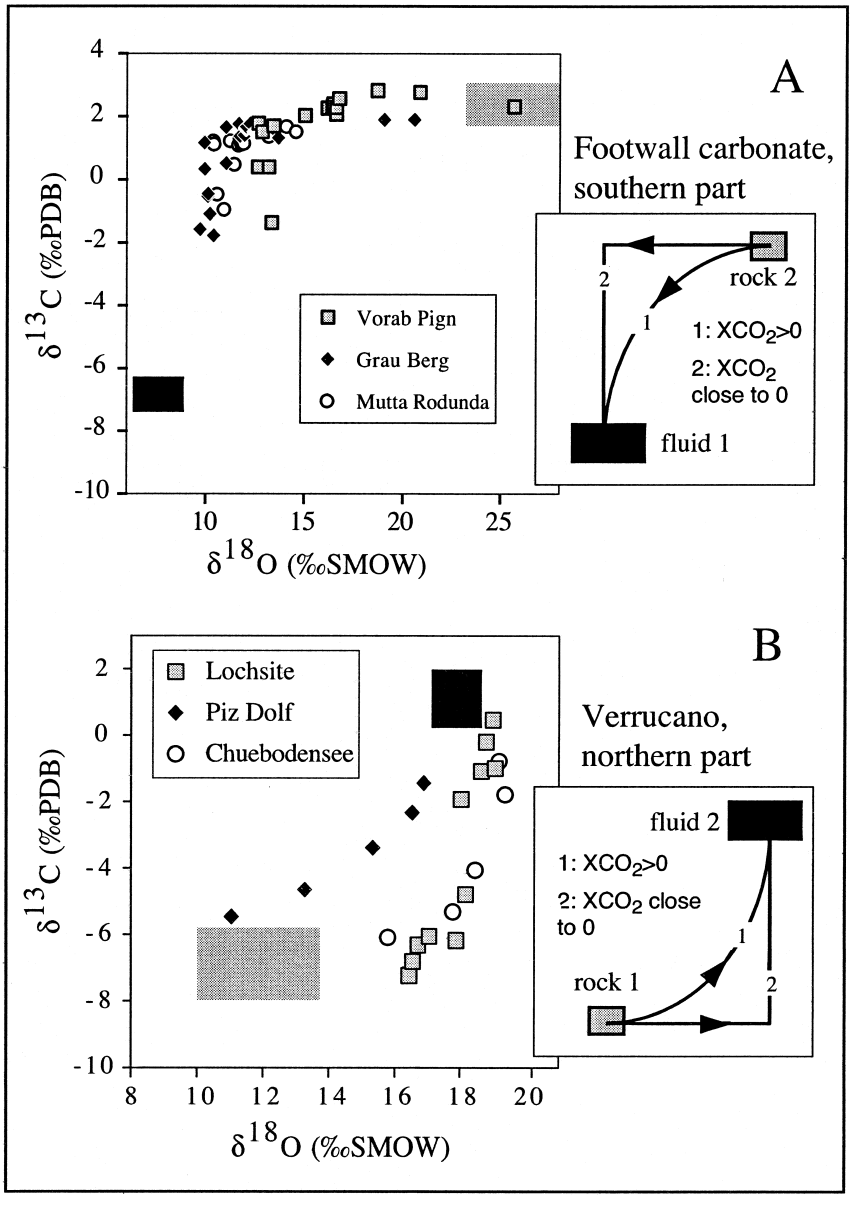

Fig. 15. (A) Isotopic composition of footwall carbonate calcite from different sites along the Glarus thrust in $\delta^{18}O$ vs. $\delta^{13}C$. Helvetic marine carbonate compositions are indicated by gray box (according to Burkhard and Kerrich, 1988). The compositions of the suspected fluid with which the carbonates interacted is indicated by a black box. The suggested exchange trend between the carbonates and a depleted external metamorphic fluid is indicated on the lower right. The exact trend depends on X_{CO_2}. With X_{CO_2} close to 0 it has a typical L shape, if X_{CO_2} increases the curve becomes smoother. (B) Isotopic composition of Verrucano calcites from different sites along the Glarus thrust in $\delta^{18}O$ versus $\delta^{13}C$. Verrucano unaltered compositions are indicated by gray box (according to Burkhard and others, 1992). The compositions of the suspected fluid with which the Verrucano interacted is indicated by a black box. The suggested exchange trend between the Verrucano and an enriched fluid is indicated on the lower right. The exact trend depends on X_{CO_2}. With X_{CO_2} close to 0 it has a typical L shape, if X_{CO_2} increases the curve becomes smoother.

TABLE 2

Fluid flow parameters in three vertical profiles

t (years)	t (s)	D (m^2/s)	υ (m/s)
10^5	$3.15X10^{12}$	1 to $4X10^{-12}$	0.7 to $1.2X10^{-10}$
10^6	$3.15X10^{13}$	1 to $4X10^{-13}$	0.7 to $1.2X10^{-11}$
10^7	$3.15X10^{14}$	1 to $4X10^{-14}$	0.7 to $1.2X10^{-12}$

Fluid flow parameters deduced from fitting curves with $\delta^{18}O$ data of calc-mylonite in three vertical profiles of the southern part of the Glarus overthrust. The calculation is based on transport theory. t is time, D is the dispersive/diffusive coefficient and υ is the mean interstitial particle velocity for the downward infiltration system that occurred in the southern part of the Glarus overthrust.

plained as a secondary calcite mineralization along this lithological/tectonic boundary. The gradient in the Verrucano can be interpreted in terms of a coupled advective and diffusive/dispersive infiltration (or advection and kinetically-controlled exchange) of ^{18}O and ^{13}C enriched Flysch-derived fluids. A scenario (fig. 12, right), where the footwall is regarded as an infinite reservoir that buffers the oxygen and carbon isotope compositions at the thrust contact (pinned boundary model according to Bickle and Baker, 1990) can be modeled if upward transport is regarded as a diffusive/dispersive process. The isotope composition is given by equation (5). The corresponding model curves fitted to our data are shown in figure 16. The inferred diffusion lengths of 2.99 meters (Piz Dolf), 6.4 meters (Chuebodensee), and 9.1 meters (Lochsite), respectively, for oxygen and 1.8 meters, 1.6 meters, 1.97 meters, respectively, for carbon increase from south to north. In other words, the upward transport component increases northward.

Another alternative is that calcite saturated fluids equilibrated with the Flysch escaped upward into the hangingwall where they lead to the formation of calcite veins. The latter would be increasingly depleted in ^{18}O and ^{13}C due a Rayleigh distillation effect (see for example, Abart and Pozzorini, 2000).

The relatively weak retardation of the carbon, with respect to the oxygen fronts may testify to relatively high C/O ratios in the pore fluid. When looking at figure 15B, we could infer $X_{CO_2} = 0.3$ at Chuebodensee and Lochsite and $X_{CO_2} = 0.4$ at Piz Dolf (see Baumgartner and Rumble, 1988). Such a high X_{CO_2} is compatible with a formation of the calc-mylonite by the precipitation of calcite veins. In the north, fluids with high X_{CO_2} and with $\delta^{18}O$ and $\delta^{13}C$ equilibrated with the Flysch are ponded below the VF, where they precipitate abundant calcite veins, before infiltrating the overlying VF.

Large Scale Isotopic Variations Within the Verrucano Formation

The increase of calcite $\delta^{18}O$ values in the Verrucano 10 meters above the thrust from 10 to 12 permil in the south to 17 permil in the north could potentially be interpreted as an even larger north-south isotope front than the one observed within the Lochsiten calc-mylonite. The entire Verrucano formation with an original calcite $\delta^{18}O$ of 17 permil could have been infiltrated by an ^{18}O depleted fluid coming from farther south and escaping to the north. In this interpretation, the southernmost $\delta^{18}O$

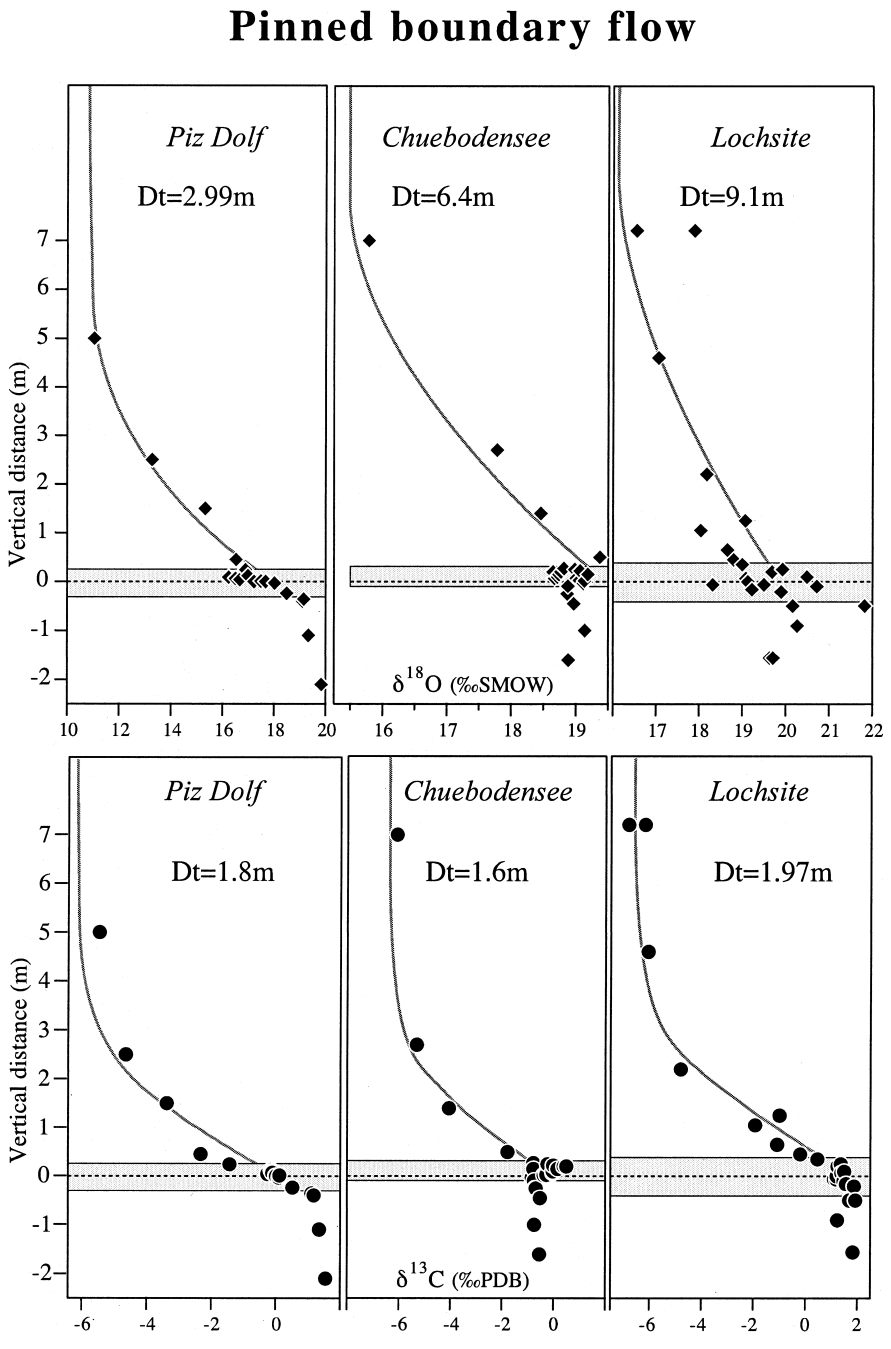

Fig. 16. Calculated curves for calcite $\delta^{18}O$ (upper part) and $\delta^{13}C$ (lower part) composition against vertical distance predicted by pinned boundary flow model of Bickle and Baker (1990) are represented together with the $\delta^{18}O$ and $\delta^{13}C$ data from three sites of the northern part of the Glarus overthrust. t is time and D is the effective oxygen dispersion/diffusion coefficient. D*t is referred to as the characteristic length of dispersion/diffusion.

of 12 permil would represent the upstream segment of an isotope front where rock is equilibrated with the fluid. However, at 100 meters above the thrust, no regional such trend can be identified in the $\delta^{18}O$ values of calcite and bulk rock (fig. 8). This relationship clearly documents that this increasing trend is due to the northwards increasing amount of infiltration of ^{18}O-enriched fluids from the footwall. This increase may be due to the thicker sequence of Flysch or to a more permeable Verrucano as it loses phyllosilicates (fig. 8).

$\delta^{18}O$ and $\delta^{13}C$ Vein Matrix Relations

Veins generally display very small differences in calcite $\delta^{18}O$ and $\delta^{13}C$ compared to their matrix (fig. 9), a relationship that could be interpreted as closed system behavior (Burkhard and Kerrich, 1988). Vein-Matrix pairs from both Verrucano and footwall carbonates, however, display very large deviations from their typical unaltered protolith composition in both $\delta^{18}O$ and $\delta^{13}C$. This contrast gives clear indication for the infiltration of external fluids into both of these rock reservoirs. These fluids were quickly rock-buffered as they traveled through these two lithologies prior to precipitating veins with an isotopic signature close to equilibrium with their immediate wall rock. Ongoing deformation and associated dynamic recrystallization must have helped to continuously re-equilibrate older matrix and vein material with new fluid batches in order to progressively enlarge the Verrucano and footwall carbonate alteration zones. In the Flysch on the other hand, a tight clustering of $\delta^{18}O$ and to a lesser degree in $\delta^{13}C$ around a typical protolith value and the absence of any isotopic gradient toward the thrust contact provides evidence for an abundant internally buffered fluid escaping upward and preventing the downard infiltration and lateral seepage of any external fluid.

$^{87}Sr/^{86}Sr$ of the Calc-mylonite

On all three rock slabs, homogeneous $^{87}Sr/^{86}Sr$ values (fig. 10) are found within a topmost zone consisting of recrystallized and strongly deformed and disrupted veins. We interpret the observed homogeneity of the $^{87}Sr/^{86}Sr$ values within this zone as due to the precipitation of veins from an externally derived fluid enriched in ^{87}Sr. The thickness of the homogeneous zone depends on the quantity of precipitated veins. At the two southern locations Fuorcla Sura and Vorab Pign, this fluid must have acquired its $^{87}Sr/^{86}Sr$ signature from either the overlying Verrucano or from basement rocks located farther south and in the footwall of the thrust. The immediate marine carbonates of the footwall are incapable of producing the observed enrichment in radiogenic ^{87}Sr. A northward decrease in mean $^{87}Sr/^{86}Sr$ values provides an argument in favor of a distant fluid source. On its way northward, this fluid would have been progressively depleted in ^{87}Sr by fluid-rock interaction with low ^{87}Sr marine carbonates in the footwall. At both sites, Fuorcla Sura and Vorab Pign, vertical downward decreasing trends in $^{87}Sr/^{86}Sr$ are indeed observed within gray mylonitized footwall carbonates. These gradients are interpreted as isotope fronts due to the downward infiltration of ^{87}Sr enriched fluids into the footwall carbonates of marine origin. The retardation of the $^{87}Sr/^{86}Sr$ front compared to that of $\delta^{18}O$ could be used to provide additional constraints on transport mechanisms and TIFF – at this stage, however, there is not enough $^{87}Sr/^{86}Sr$ data available to provide a sound basis for such a modeling attempt. At the northern Sardona site, we were unable to detect any systematic vertical trend on a slab with more than 15 centimeters width. This lack in trend is attributed to the fact that the analyzed slab of calc-mylonite consists mostly of secondary vein calcite with a very chaotic “foliated gauge” texture and mechanical mixing of calcite could have strongly contributed to the homogenization of the $^{87}Sr/^{86}Sr$ values. Furthermore the $^{87}Sr/^{86}Sr$ signature at Sardona does not allow for a

discrimination between fluids channelized along the thrust and fluids coming out of the underlying Flysch which in itself may be a source for a slight ^{87}Sr- enrichment.

Insights Into the Origin and Formation of Lochsiten Calc-mylonite

The origin of the Lochsiten calc-mylonite layer has puzzled geologists for over 150 years and still is a matter of debate. In the classic view (see for example, Heim 1921, p. 10 ff.), this layer represents an extremely thinned out inverted limb of a recumbent fold, connecting Mesozoic carbonates in the Helvetic nappes of the hangingwall with similar carbonates of the Infrahelvetic complex in the footwall. Superplastic behavior has been postulated in order to explain the apparent weakness of this limestone thrust horizon and its extreme thinning without necking (Schmid, Boland, and Paterson, 1977). Based on isotopic and structural observations made within the Lochsitenkalk-mylonite this now widely accepted view has recently been questioned again (Burkhard and others 1992; Badertscher and Burkhard, 2001). Earlier extreme views include Rothpletz's (1883) who interpreted the entire (brittle) thrust fault as being mineralized by secondary calcite. Detailed isotopic measurements presented here provide new constraints to this old question. In the northern areas, where Verrucano is overriding Flysch in the footwall, the Lochsitenkalk mylonite with a thickness between 0.5 and 5 meters appears to be predominantly made of a pile of intricately folded and disrupted veins separated from each other by dark stylolitic seams. There is little if any structural and no isotopic evidence for a marine carbonate origin of the calc-mylonite at these northern sites. Further south, however, two different types of mylonites are distinguishable. Within the topmost few meters to decimeters, increasingly mylonitized carbonates are clearly derived from the underlying Mesozoic footwall rocks. Here, "true" Lochsitenkalk of secondary, vein origin (in our narrow definition) is restricted to a thin but continuous band of 5 to 15 centimeters thickness, separating the Verrucano hangingwall from the footwall. The same observation can be made at the top of carbonate thrust slices with dimensions of 10's to 100's of meters, occasionally found immediately below the thrust contact, apparently dragged over some kilometers northward on top of Flysch.

CONCLUSIONS

In the Glarus area, fluid flow pathways have been derived from stable and Sr-isotope systematics (fig. 17). Two regions of different flow regimes, approximately separated by the carbonate/Flysch boundary in the footwall, have been documented. South of the carbonate/Flysch boundary, externally derived fluids were strongly channelized along the thrust in a general northward direction of flow (Burkhard and others 1992; McCaig and others, 1995). These fluids, with an initial $\delta^{18}O$ of 6 to 10 permil have been transported by a coupled advective and dispersive/diffusive process and lead to a pronounced large-scale oxygen isotope front within the calc-mylonite. A Pecklet number N_{Pe} of 12.8 to 39.5 for this flow system documents a highly dispersive/diffusive transport mechanism. The characteristic length of dispersion/diffusion of 0.36 to 2.3 kilometers cannot be accounted for by molecular diffusion alone and hence hydrodynamic dispersion is inferred to have played a major role (compare Bowman, Willett, and Cook, 1994). The regional trend of ^{18}O signature of the calc-mylonite may have been significantly influenced also by cross thrust transport components (Abart and others, 2002). Observed ^{18}O and ^{13}C enrichments within the lowermost 50 to 100 centimeters of the hangingwall Verrucano are interpreted as due to transversal hydrodynamic dispersion, mainly accommodated by fracture flow which lead to the addition of secondary calcite in the form of veinlets (Abart and others, 2002). In the footwall carbonates, $\delta^{18}O$, $\delta^{13}C$ and $^{87}Sr/^{86}Sr$ gradients are recognized as isotopic fronts due to the downward infiltration of fluids with $\delta^{18}O$ of about 7 permil, $\delta^{13}C$ of –5 permil, $^{87}Sr/^{86}Sr > 0.715$ and a $X_{CO_2} = 0.1$ in apparent equilibrium with overlying

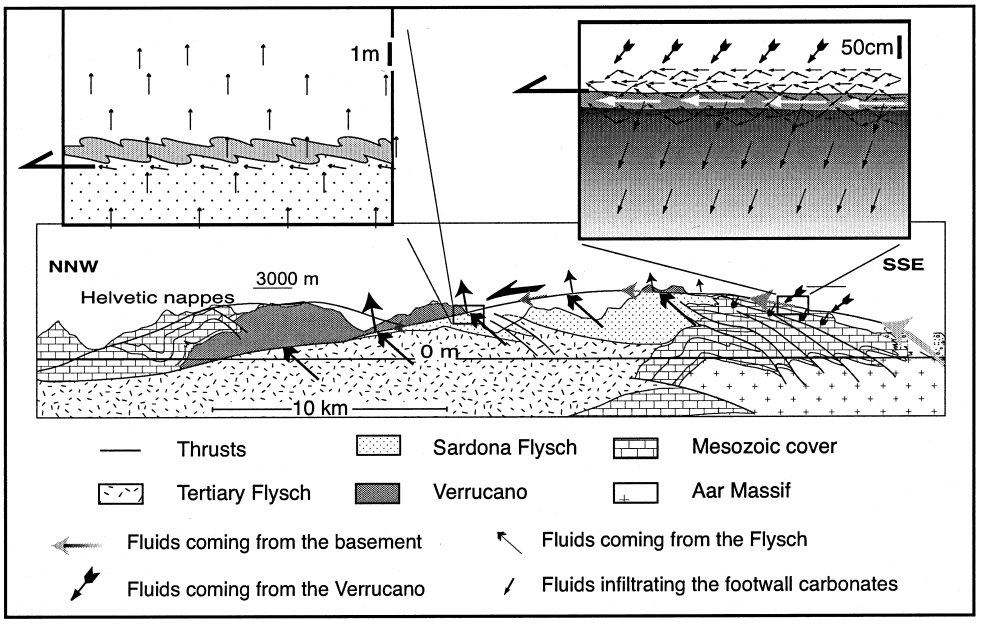

Fig. 17. Cross section of the Glarus Alps in eastern Switzerland (according to Oberholzer, 1933) on which are indicated the different flow systems (arrows). Two close-up views are given to show the details of the fluid flow patterns at the thrust contact. The size of arrows is proportional to the suspected flux of a particular flow system.

Verrucano rocks. A downward directed TIFF of 3.45 to 5.7 m^3/m^2 is calculated from the shape of isotopic profiles, indicating that the cross thrust, downward infiltration is three orders of magnitudes smaller than the channelized south-north flow component, for which a TIFF of 4500 to 9100 m^3/m^2 has been obtained. In our preferred fluid flow model, the downward gradients are therefore interpreted as lateral seepage of an important channelized northward flow of fluids originating from a more distant "metamorphic" source.

In the northern areas, calcite $\delta^{18}O$ values of the calc-mylonite are strongly clustered around 20 permil, in apparent equilibrium with underlying Flysch, but far from the isotopic composition of a supposed Mesozoic carbonate protolith (25 permil). In terms of isotopic signatures, this part of the thrust cannot be simply interpreted as the downstream segment of channelized flow as previously proposed (Burkhard and others 1992; Bowman, Willett, and Cook, 1994). Vertical isotope profiles into the overlying Verrucano hangingwall require a strong upward fluid flow component (Abart and others, 2002). The obvious source are calcite saturated fluids in equilibrium with the dewatering Flysch escaping upward and forelandward (Marquer and Burkhard, 1992; Oliver, 1986). Such fluids are responsible for the precipitation of abundant veins at the thrust contact, leading to the precipitation of a meter thick accumulation of secondary calcite in the form of Lochsitenkalk with a regionally almost constant $\delta^{18}O$ and $\delta^{13}C$ signature. Ongoing, alternating brittle and ductile deformation of this layer is responsible for the formation of a conspicuous "foliated gouge" texture of this Lochsitenkalk (Badertscher and Burkhard, 2001). Flysch derived fluids with a $\delta^{18}O$ of about 15 permil, an initial $\delta^{13}C$ of about. + 2 permil and a X_{CO_2} = 0.3 to 0.4 infiltrated the hangingwall, where a decreasing number of calcite veinlets are responsible for an alteration zone extending several meters upward into

the Verrucano Formation. Upward decreasing $\delta^{13}C$ values are interpreted as due to a Rayleigh type fractionation associated with a progressive decrease in X_{CO_2} of the infiltrating fluid. This important additional fluid source obscures any isotopic signature of the thrust parallel fluid flow identified further south. Most likely, however, channelized flow along the thrust was confined to the deeper, southernmost parts of the Glarus thrust while a general upward dissipation of these same fluids into the hangingwall seems to have occurred further north.

ACKNOWLEDGMENTS

We would like to thank Stephen Burns and Bob Cliff for their help during data acquisition and Nathalie Challandes, François Gainon and Alexandre Aubry for their assistance during field campaigns. Nicolas Badertscher wants to thank particularly "El Professore" for his help during all this work. Bruce Yardley and Edward Bolton are acknowledged for their constructive reviews. This research was funded by the Swiss National Science Foundation grants no. 20–50535.97 and no. 20–56920.99.

References

Abart, R., Badertscher, N., Burkhard, M., and Podoven, E., 2002, Oxygen, carbon and strontium isotope systematics in two profiles across the Glarus thrust: implications for fluid flow: Contributions to Mineralogy and Petrology, v. 143, p.192-208.

Abart, R., and Pozzorini, D., 2000, Implications of kinetically controlled mineral-fluid exchange on the geometry of stable-isotope fronts: European Journal of Mineralogy, v. 12, p. 1069-1082.

Abart, R., and Sperb, R., 1997, Grain-scale stable isotope disequilibrium during fluid-rock interaction; 1, Series approximations for advective-dispersive transport and first-order kinetic mineral-fluid exchange: American Journal of Science, v. 297, p. 679-706.

Badertscher, N. P., and Burkhard, M., 2001, Brittle-Ductile deformations in the Glarus thrust Lochseiten (LK) calc-mylonite: Terra Nova, v. 12, p. 281-288.

Baker, J., and Spiegelman, M., 1995, Modeling an infiltration-driven geochemical front: Earth and Planetary Science Letters, v. 136, p. 87-96.

Baumgartner, L. P., and Rumble, D., 1988, Transport of stable isotopes; 1, Development of a kinetic continuum theory for stable isotope transport: Contributions to Mineralogy and Petrology, v. 98, p. 417-430.

Bickle, M. J., and Baker, A. J., 1990, Advective-diffusive transport of isotopic fronts: an example from Naxos, Greece: Earth and Planet Science Letters, v. 97, p. 78-93.

Bickle, M. J., and McKenzie, D., 1987, The transport of heat and matter by fluids during metamorphism: Contributions to Mineralogy and Petrology, v. 95, p. 384-392.

Bowman, J. R., Willett, S. D., and Cook, S. J., 1994, Oxygen isotopic transport and exchange during fluid flow; one-dimensional models and applications: American Journal of Science, v. 294, p. 1-55.

Burkhard, M., and Kerrich, R., 1988, Fluid regimes in the deformation of the Helvetic Nappes, Switzerland, as inferred from stable isotope data: Contributions to Mineralogy and Petrology, v. 99, p. 416-429.

——— 1990, Fluid-rock interactions during thrusting of the Glarus Nappe; evidence from geochemical and stable isotope data: Schweizerische Mineralogische und Petrographische Mitteilungen: Bulletin Suisse de Minéralogie et Pétrographie, v. 70, p. 77-82.

Burkhard, M., Kerrich, R., Maas, R., and Fyfe, W. S., 1992, Stable and Sr-isotope evidence for fluid advection during thrusting of the Glarus nappe (Swiss Alps): Contributions Mineralogy Petrology, v. 112, p. 293-311.

Cathless, L. M., III, 1990, Scales and effects of fluid flow in the upper crust: Science, v. 248, p. 323-329.

Clayton, R. N., Goldsmith, J. R., and Mayeda, T. K., 1989, Oxygen isotope fractionation in quartz, albite, anorthite and calcite: Geochimica et Cosmochimica Acta, v. 53, p. 725-733.

Cox, S. F., 1987, Antitaxial crack-seal vein microstructures and their relationship to displacement paths: Journal of Structural Geology, v. 9, p. 779-787.

Cox, S. F., and Etheridge, M. A., 1989, Coupled grain-scale dilatancy and mass transfer during deformation at high fluid pressures; examples from Mount Lyell, Tasmania: Journal of Structural Geology, v. 11, p. 147-162.

Crank, J., 1975, The Mathematics of Diffusion: Oxford, Clarendon press, 347 p.

Crespo-Blanc, A., Masson, H., Sharp, Z., Cosca, M., and Hunziker, J., 1995, A stable and $^{40}Ar/^{39}Ar$ isotope study of a major thrust in the Helvetic nappes (Swiss Alps); evidence for fluid flow and constraints on nappe kinematics: Geological Society of America Bulletin, v. 107, p. 1129-1144.

Dipple, G. M., and Ferry, J. M., 1992, Metasomatism and fluid flow in ductile fault zones: Contributions to Mineralogy and Petrology, v. 112, p. 149-164.

Eppel, H., and Abart, R., 1997, Grain-scale stable isotope disequilibrium during fluid-rock interaction; 2, An example from the Penninic-Austroalpine tectonic contact in eastern Switzerland: American Journal of Science, v. 297, p. 707-728.

Etheridge, M. A., Wall, V. J., Cox, S. F., and Vernon, R. H., 1984, High fluid pressures during regional metamorphism and deformation; implications for mass transport and deformation mechanisms: Journal of Geophysical Research, v. 89, p. 4344-4358.

Etheridge, M. A., Wall, V. J., and Vernon, R. H., 1983, The role of the fluid phase during regional metamorphism and deformation: Journal of Metamorphic Geology, v. 1, p. 205-226.

Ferrero, J., 1965, Dosage des principaux minéraux des roches par diffraction de Rayons X: Rapport C.F.P. (Bordeaux), inédit.

——— 1966, Nouvelle méthode empirique pour le dosage des minéraux par diffraction R.X.: Rapport C.F.P. (Bordeaux), inédit.

Franck, E. U., Wiegand, G., and Dahmen, N., 1996, Water, *in* Ullmann's Encyclopedia of Industrial Chemistry: Weinheim, Verlag Chemie, v. 28A, p. 12.

Frey, M., 1988, Discontinuous inverse metamorphic zonation, Glarus Alps, Switzerland; evidence from illite "crystallinity" data: Schweizerische Mineralogische und Petrographische Mitteilungen: Bulletin Suisse de Mineralogie et Petrographie, v. 68, p. 171-183.

Fyfe, W. S., and Kerrich, R., 1985, Fluids and thrusting: Chemical Geology, v. 49, p. 353-362.

Groshong, R. H., Jr., Pfiffner, O. A., and Pringle, L. R., 1984, Strain partitioning in the Helvetic thrust belt of eastern Switzerland from the leading edge to the internal zone: Journal of Structural Geology, v. 6, p. 5-18.

Heim, A., 1921, Geologie der Schweiz, Bd. II. Tauchniz, Leipzig, 476 p.

Hsu, K. J., 1969, A preliminary Anlysis of the Statics and Kinetics of the Glarus Overthrust: Eclogae geologica Helvetiae, v. 62, p. 143-154.

Hubbert, M. K., and Rubey, W. W., 1959, Role of fluid pressure in mechanics of overthrust faulting: Geological Society of America Bulletin, v. 70, p. 115-166.

Hunziker, J. C., Frey, M., Clauer, N., Dallmeyer, R. D., Friedrichsen, H., Flehmig, W., Hochstrasser, K., Roggwiler, P., and Schwander, H., 1986, The evolution of illite to muscovite; mineralogical and isotopic data from the Glarus Alps, Switzerland: Contributions to Mineralogy and Petrology, v. 92, p. 157-180.

Kerrich, R., La Tour, T. E., and Willmore, L., 1984, Fluid Participation in Deep Fault Zones; Evidence from Geological, Geochemical, and $^{18}O/^{16}O$ Relations, *in* Kirby, S. H., and Scholz, C. H., editors, Chemical Effects of Water on the Deformation and Strengths of Crustal Rocks: Journal of Geophysical Research, v. 89, p. 4331-4343.

Kirschner, D. L., Masson, H., and Sharp, Z. D., 1999, Fluid migration through thrust faults in the Helvetic nappes (Western Swiss Alps): Contributions to Mineralogy and Petrology, v. 136, p. 169-183.

Klug, H. P., and Alexander, L. E., 1974, X-ray Diffraction Procedures: For Polycrystalline and Amorphous Materials: New York, J. Wiley & Sons, 992 p.

Knipe, R. J., and McCaig, A. M., 1994, Microstructural and microchemical consequences of fluid flow in deforming rocks, *in* Parnell, J. E., editor, Geofluids; origin, migration and evolution of fluids in sedimentary basins: London, Geological Society of London, Geological Society Special Publications, no. 78, p. 99-111.

Kübler, B., 1983, Dosage quantitatif des minéraux majeurs des roches sédimentaires par Diffractzion X.: Cahier de l'Institut de Géologie de Neuchâtel, v. Série AX N°1.1 & 1.2.

Lassey, K. R., and Blattner, P., 1988, Kinetically controlled oxygen isotope exchange between fluid and rock in one-dimensional advective flow: Geochimica et Cosmochimica Acta, v. 52, p. 2169-2175.

Marquer, D., and Burkhard, M., 1992, Fluid circulation, progressive deformation and mass-transfer processes in the upper crust; the example of basement-cover relationships in the External Crystalline Massifs, Switzerland: Journal of Structural Geology, v. 14, p. 1047-1057.

McCaig, A. M., 1984, Fluid-rock interaction in some shear zones from the Pyrenees: Journal of Metamorphic Geology, v. 2, p. 129-141.

——— 1989, Geology; fluid flow through fault zones: London, Nature, v. 340, p. 600.

——— 1997, The geochemistry of volatile fluid flow in shear zones, *in* Holness, M. B., editor, Deformation-enhanced Fluid Transport in the Earth's Crust and Mantle: London, Chapman & Hall, p. 227-266.

McCaig, A. M., Wickham, S. M., and Taylor, H. P., Jr., 1990, Deep fluid circulation in Alpine shear zones, Pyrenees, France; field and oxygen isotope studies: Contributions to Mineralogy and Petrology, v. 106, p. 41-60.

McCaig, A. M., Wayne, D. M., Marshall, J. D., Banks, D., and Henderson, I., 1995, Isotopic and fluid inclusion studies of fluid movement along the Gavarnie Thrust, central Pyrenees; reaction fronts in carbonate mylonites: American Journal of Science, v. 295, p. 309-343.

McCaig, A. M., Tritlla, J., and Banks, D. A., 2000, Fluid mixing and recycling during Pyrenean thrusting: Evidence from fluid inclusion halogen ratios: Geochimica et Cosmochimica Acta, v. 64, p. 3394-3412.

Oberholzer, J., 1933, Geologie der Glarner Alpen, Beiträge Geologische Karte Schweiz: Geologische Kommission.

Oliver, J., 1986, Fluids expelled tectonically from orogenic belts; their role in hydrocarbon migration and other geologic phenomena: Geology (Boulder), v. 14, p. 99-102.

Oliver, N. H. S., 1996, Review and classification of structural controls on fluid flow during regional metamorphism: Journal of Metamorphic Geology, v. 14, p. 477-492.

Oliver, N. H. S., Valenta, R. K., and Wall, V. J., 1990, The effect of heterogeneous stress and strain on metamorphic fluid flow, Mary Kathleen, Australia, and a model for large-scale fluid circulation: Journal of Metamorphic Geology, v. 8, p. 311-331.

O'Neil, J. R., Clayton, R. N., and Mayeda, T. K., 1969, Oxygen isotope fractionation in divalent metal carbonates: The Journal of Chemical Physics, v. 51, p. 5547-5558.

Pfiffner, O. A., 1977, Tektonische Untersuchungen im Infrahelvetikum der Ostschweiz. Translated title: Tectonic studies of the Infrahelvetic Complex, eastern Switzerland: Zuerich, University, Geologisches Institut Eidgenoessische Technische Hochschule, Geololgisches Institut Mitteilungen, v. 217, p. 164.

——— 1981, Fold- and -thrust tectonics in the Helvetic Nappes (E. Switzerland), *in* McClay, K. R. and Price, R., editor, Thrust and Nappe Tectonics: London, The Geological Society of London, Special Publication Geological Society of London, no. 9, p. 319-327.
——— 1985, Displacements along thrust faults: Eclogae-Geologicae-Helvetiae, v. 78, p. 313-333.
——— 1993, The structure of the Helvetic nappes and its relation to the mechanical stratigraphy: Journal of Structural Geology, v. 15, p. 511-521.
Price, R. A., 1988, The mechanical paradox of large overthrusts: Geological Society of America Bulletin, v. 100, p. 1898-1908.
Rahn, M., Mullis, J., Erdelbrock, K., and Frey, M., 1995, Alpine metamorphism in the North Helvetic flysch of the Glarus Alps, Switzerland: Eclogae Geologicae Helvetiae, v. 88, p. 157-178.
Rolli, M., 1990, Dosage semi-quantitatif RX sur Scintag.: Cahiers de l'Institut de Géologie de Neuchâtel, Suisse, v. Série ADX, 1-49.
Rothpletz, A.,1883, Der Gebirgsbau der Alpen beiderseits des Rheines. Zeitschrift der Deutschen geologie Ges., p. 167-168.
Sample, J. C., 1996, Isotopic evidence from authigenic carbonates for rapid upward fluid flow in accretionary wedges: Geology (Boulder), v. 24, p. 897-900.
Schmid, S. M., 1975, The Glarus overthrust; field evidence and mechanical model: Eclogae Geologicae Helvetiae, v. 68, p. 247-280.
Schmid, S. M., Boland, J. M., and Paterson, M. S., 1977, Superplastic flow in fine grained limestone: Tectonophysics, v. 43, p. 257-291.
Schmid, S. M., Pfiffner, O. A., Schönborn, G., Frotzheim, N., and Kissling, E., 1997, Integrated cross section and tectonic evolution of the Alps along the Eastern Traverse, *in* Pfiffner, O. A., Lehner, P., Heitzmann, P., Mueller, S., and A., S., editors, Deep Structure of the Swiss Alps: Basel, Birkhäuser Verlag, p. 289-304.
Sharp, Z. D., 1990, A laser-based microanalytical method for the *in situ* determination of oxygen isotope ratios of silicates and oxides: Geochimica et Cosmochimica Acta, 54, p. 1353-1357.
Silver, E., Kastner, M., Fisher, A., Morris, J., McIntosh, K., and Saffer, D., 2000, Fluid flow paths in the Middle America Trench and Costa Rica margin: Geology, v. 28, p. 679-682.
Valley, J.W., Kitchen, N., Kohn, M. J., Niendorf, C. R., Spicuzza, M. J., 1995, UWG-2, a garnet standard for oxygen isotope ratios; strategies for high precision and accuracy with laser heating: Geochimica et Cosmochimica Acta, 59, p. 5223-5231.
Yardley, B. W. D., and Lloyd, G. E., 1995, Why metasomatic fronts are really metasomatic sides: Geology (Boulder), v. 23, p. 53-56.